Since January 2020 Elsevier has created a COVID-19 resource centre with free information in English and Mandarin on the novel coronavirus COVID-19. The COVID-19 resource centre is hosted on Elsevier Connect, the company's public news and information website.

Article

Cell

Mycobacterium tuberculosis Sulfolipid-1 Activates Nociceptive Neurons and Induces Cough

Graphical Abstract

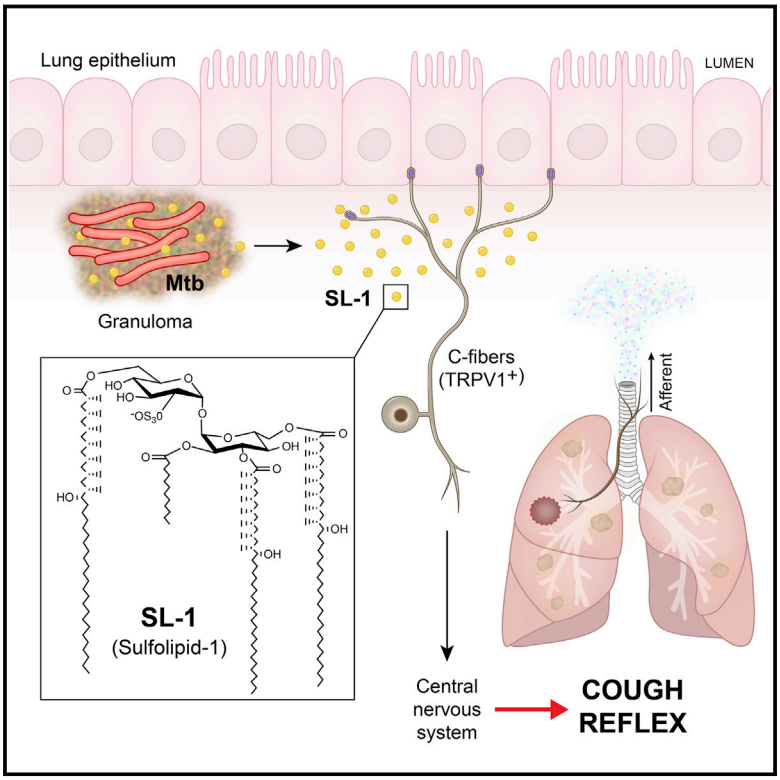

Authors

Cody R. Ruhl, Breanna L. Pasko, Haaris S. Khan, ..., Gregory Dussor, Theodore J. Price, Michael U. Shiloh

Correspondence

michael.shiloh@utsouthwestern.edu

In Brief

Mycobacterium tuberculosis produces a glycolipid called sulfolipid-1 (SL-1) that triggers cough by activating nociceptive neurons.

Highlights

- An Mtb organic extract activates nociceptive neurons and induces cough in guinea pigs
- Mtb sulfolipid-1 is necessary and sufficient to trigger neuronal activation and cough
- Guinea pigs infected with an SL-1-deficient Mtb mutant do not cough

Ruhl et al., 2020, Cell *181*, 293–305
April 16, 2020
https://doi.org/10.1016/j.cell.2020.02.026

CellPress

Article

Cell

Mycobacterium tuberculosis Sulfolipid-1 Activates Nociceptive Neurons and Induces Cough

Cody R. Ruhl,[1] Breanna L. Pasko,[1] Haaris S. Khan,[1] Lexy M. Kindt,[1] Chelsea E. Stamm,[1] Luis H. Franco,[1,7] Connie C. Hsia,[1] Min Zhou,[2] Colton R. Davis,[2] Tian Qin,[2] Laurent Gautron,[1,3] Michael D. Burton,[4,5] Galo L. Mejia,[4,5] Dhananjay K. Naik,[4,5] Gregory Dussor,[4,5] Theodore J. Price,[4,5] and Michael U. Shiloh[1,6,8,*]

[1]Department of Internal Medicine, University of Texas Southwestern Medical Center, Dallas, TX 75390, USA
[2]Department of Biochemistry, University of Texas Southwestern Medical Center, Dallas, TX 75390, USA
[3]Center for Hypothalamic Research, University of Texas Southwestern Medical Center, Dallas, TX 75390, USA
[4]School of Behavioral and Brain Sciences, University of Texas at Dallas, Richardson, TX 75080, USA
[5]Center for Advanced Pain Studies, University of Texas at Dallas, Richardson, TX 75080, USA
[6]Department of Microbiology, University of Texas Southwestern Medical Center, Dallas, TX 75390, USA
[7]Present address: Departamento de Bioquímica e Imunologia, Universidade Federal de Minas Gerais, Belo Horizonte 30270-901, Brazil
[8]Lead Contact
*Correspondence: michael.shiloh@utsouthwestern.edu
https://doi.org/10.1016/j.cell.2020.02.026

SUMMARY

Pulmonary tuberculosis, a disease caused by *Mycobacterium tuberculosis* (Mtb), manifests with a persistent cough as both a primary symptom and mechanism of transmission. The cough reflex can be triggered by nociceptive neurons innervating the lungs, and some bacteria produce neuron-targeting molecules. However, how pulmonary Mtb infection causes cough remains undefined, and whether Mtb produces a neuron-activating, cough-inducing molecule is unknown. Here, we show that an Mtb organic extract activates nociceptive neurons *in vitro* and identify the Mtb glycolipid sulfolipid-1 (SL-1) as the nociceptive molecule. Mtb organic extracts from mutants lacking SL-1 synthesis cannot activate neurons *in vitro* or induce cough in a guinea pig model. Finally, Mtb-infected guinea pigs cough in a manner dependent on SL-1 synthesis. Thus, we demonstrate a heretofore unknown molecular mechanism for cough induction by a virulent human pathogen via its production of a complex lipid.

INTRODUCTION

A hallmark symptom of active pulmonary tuberculosis and a major mechanism of disease transmission is a persistent, sometimes bloody cough. The vast majority of *de novo Mycobacterium tuberculosis* (Mtb) infections are acquired from contact with actively infected, coughing individuals (Fennelly et al., 2004; Jones-López et al., 2015). Previous hypotheses regarding the mechanism of cough in pulmonary tuberculosis emphasized the role of infection-induced lung irritation and production of inflammatory mediators (Turner, 2019; Turner and Bothamley, 2015). However, empiric evidence for these hypotheses is lacking. We generated an alternative hypothesis that Mtb produces a cough-triggering molecule, thereby enhancing its own transmission.

The cough reflex, which may have evolved as a defense against aspiration of food and gastric contents or inhalation of irritants and infectious particles, is a complex, highly organized, neuromuscular response conserved across mammalian species (Brooks, 2011; Canning, 2008, 2010). Chemosensory afferent neurons innervating the upper airway and lungs respond to a variety of chemicals, including exogenous noxious molecules like capsaicin, particulates, and cigarette smoke (Mazzone, 2005; Mazzone and Undem, 2016). Such neurons have been directly visualized in whole mount biopsies of mouse, rat, guinea pig, and human lungs (De Proost et al., 2007a, 2007b; Pintelon et al., 2007), where their peripheral terminals encode both ion channel and G-protein-coupled chemosensory receptors (Mazzone, 2005; Mazzone and Undem, 2016). While pulmonary defense against and response to respiratory infection is considered a major function of the cough reflex, whether virulence molecules from cough-inducing pathogens directly stimulate airway afferent neurons is unknown (Cherry, 2013; Hewlett et al., 2014; Turner and Bothamley, 2015).

Recently, diverse species of bacteria have been shown to directly stimulate peripheral nerves. For example, by producing molecules that act on nerve receptors, *Staphylococcus aureus* causes pain (Chiu et al., 2013) while *Mycobacterium ulcerans,* a species related to Mtb, causes peripheral anesthesia through interaction of the polyketide mycolactone with neurons (Marion et al., 2014).

Because Mtb is mainly a respiratory pathogen that is predominantly transmitted via cough, cough is initiated by nociceptive neurons (Canning, 2007), and bacteria are capable of altering neuronal activity, we hypothesized that Mtb produces a molecule to stimulate cough through activation of respiratory nociceptive neurons thereby facilitating its spread from infected to uninfected individuals. To test this hypothesis, we first demonstrated that guinea pigs with pulmonary tuberculosis cough, and that an organic-phase extract of Mtb consisting primarily of lipid components of its cell wall and fat-soluble molecules is sufficient to

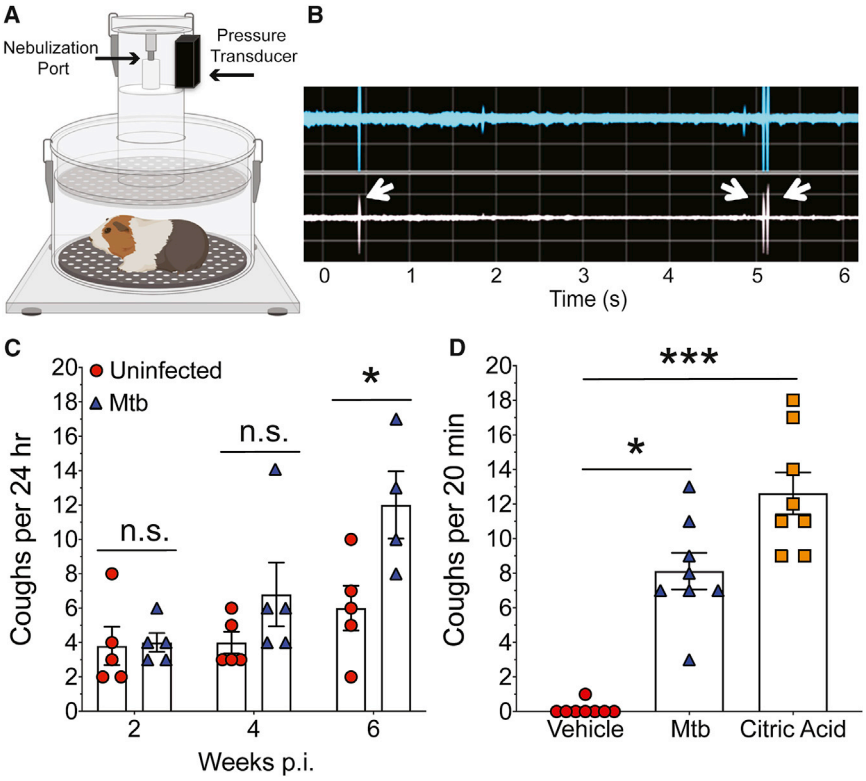

Figure 1. Mtb Infection and Mtb Extract Provoke Guinea Pig Coughs

(A) Schematic of WBP chamber.

(B) Representation of output reading from WBP including bias flow (blue) and bias flow slope (white). Arrows indicate coughs.

(C) Cough quantification over a 24 h period every 2 weeks in uninfected and Mtb-infected guinea pigs. Error bars are SEM. *p < 0.05 by Mann-Whitney U test.

(D) Triggered coughs over a 20-min period in naive, unrestrained guinea pigs after treatment with vehicle (10% MeOh in PBS), WT Erdman Mtb extract (20 mg/mL), or citric acid (0.4 M). Each point represents an individual animal exposed to vehicle, Mtb extract, and citric acid on alternating days. Error bars are SEM. *p < 0.05, ***p < 0.001 by Friedman's test.

induce cough. Exposing nociceptive neurons *in vitro* to the Mtb extract provokes a rapid increase in intracellular calcium, similar to the nociceptive molecule capsaicin. We determined that the active molecule in the Mtb extract is the mycobacterial lipid sulfolipid-1 (SL-1), an important component of the Mtb cell wall (Goren, 1970a, 1970b; Goren et al., 1971; Schelle and Bertozzi, 2006). Genetic disruption of SL-1 biosynthesis results in an Mtb extract that cannot trigger neurons *in vitro* or induce cough in guinea pigs. Finally, we find that guinea pigs infected with Mtb mutants lacking SL-1 synthesis fail to cough. This work represents the identification of a cough-inducing molecule from a virulent human pathogen, with major implications for the pathogenesis and transmission of tuberculosis.

RESULTS

Mtb Infection Induces Cough in Guinea Pigs

To determine if Mtb produces molecules that induce cough, we first established animal models of coughing, both during Mtb infection and with isolated organic Mtb extracts. Guinea pigs have long been used as a model for Mtb infection (Koch, 1912; Lurie, 1930d; Orme and Ordway, 2016; Perla, 1927) and as an established experimental model to test isolated compounds for cough induction (Laude et al., 1993; Tanaka and Maruyama, 2005; Zaccone et al., 2016). Although it was demonstrated 100 years ago that guinea pigs can transmit Mtb from infected to naive animals (Koch, 1912; Lurie, 1930a, 1930b, 1930c; Perla, 1927), to date, no studies have reported whether guinea pigs cough in the context of Mtb infection. Thus, to first assess if guinea pigs with pulmonary tuberculosis cough, we infected outbred Hartley guinea pigs with the Mtb Erdman strain via aerosol and measured cough over 24 h using whole-body plethysmography (WBP) (Morice et al., 2007; Zaccone et al., 2016). We infected guinea pigs with ~200 colony-forming units (CFU) of Mtb, placed individual animals in WBP chambers for 24 h every 2 weeks and monitored cough events by plethysmography (Figures 1A and 1B). Coughs were quantified using a pressure transducer attached to the WBP chamber (Figure 1A). Each cough was automatically identified by a predetermined algorithm based on the box flow pattern (sharp increase and decrease of box flow) that measures the sharp inspiration and expiration of air during a cough (Figure 1B). Uninfected control and Mtb-infected guinea pigs showed no statistically significant difference in coughs at 2- or 4-weeks post infection. However, at 6 weeks post-infection, Mtb-infected guinea pigs had twice as many coughs (mean 12 versus 6) compared to control guinea pigs (Figure 1C). Thus, Mtb-infected guinea pigs have more coughs than uninfected animals 6 weeks after low-dose infection, at a time of maximal lung CFU (Basaraba et al., 2006; Orme and Ordway, 2016; Turner et al., 2003).

An Organic Extract of Mtb Is Sufficient to Induce Cough in Guinea Pigs

To determine if Mtb produces a mediator of neuronal activation and cough, we performed a Folch extraction (Folch et al., 1957) from Mtb grown in liquid culture to extract polar and non-polar lipids and tested if the organic phase of the extract (hereafter called "Mtb extract") alone was sufficient to induce cough. We chose the organic fraction because the polyketide mycolactone of *M. ulcerans* is also isolated via chloroform: methanol extraction (George et al., 1998) and because Mtb has a lipid and organic metabolite rich cell wall with many active molecules (Jankute et al., 2015). We then used an established model of cough induction, namely, transient exposure of unrestrained, naive, healthy guinea pigs to noxious molecules (Laude et al.,

1993; Tanaka and Maruyama, 2005) via a nebulizer and WBP analysis to test if the Mtb extract could trigger cough. As an independent control, we exposed guinea pigs to 0.4 M citric acid, a known cough agonist (Laude et al., 1993; Morice et al., 2007). After compound nebulization, we quantified coughs over 20 min as previously reported (Laude et al., 1993; Tanaka and Maruyama, 2005; Zaccone et al., 2016). Each animal was exposed to vehicle control, Mtb extract, or citric acid on alternating days separated by a rest day to avoid tachyphylaxis. Nebulization of the vehicle control for the Mtb extract did not trigger coughing, while exposure to the Mtb extract (20 mg/mL final) produced more coughs (mean 8 versus 0.5 coughs in vehicle controls) (Figure 1D). As expected, nebulization of 0.4 M citric acid resulted in a mean of 12 coughs in 20 min (Figure 1D). Thus, an Mtb organic-phase extract induces cough in guinea pigs.

Mtb Organic Extract Activates Nociceptive Neurons *In Vitro*

Having established that the Mtb extract alone is sufficient to induce cough, we next investigated if the Mtb extract activates nociceptive neurons in cell culture using live cell imaging of intracellular calcium dynamics. When nociceptive neurons are triggered by nociceptive agonists, they demonstrate an increase in intracellular [Ca^{2+}] (Glaser et al., 2016) that can be quantified using Ca^{2+} responsive dyes (Grynkiewicz et al., 1985; Iatridou et al., 1994; Kao et al., 2010). To first determine if the Mtb extract can trigger neurons, we used the immortalized mouse embryonic dorsal root ganglion (DRG) cell line, MED17.11, which demonstrates properties of nociceptive neurons (Doran et al., 2015). We loaded MED17.11 cells with the fluorescent semiquantitative Ca^{2+} dye Fluo-4 and monitored fluorescence using live cell imaging after exposure to either vehicle control, Mtb extract, or capsaicin, a known transient receptor potential cation channel subfamily V member 1 (TRPV1) agonist (Caterina et al., 1997). After treatment with either the positive control capsaicin or the Mtb extract, we observed maximum intracellular [Ca^{2+}] responses at ~45 s, with the fluorescence returning to baseline by 90 s (Figure 2A; Video S1). We quantified the maximum change in fluorescence for each individual cell in the field of view using ImageJ and then averaged the response (Figure 2B). Not every cell responded to the Mtb extract or capsaicin, suggesting that the differentiated MED17.11 cells may not be a uniform population. However, in contrast to the vehicle control (DMSO), both Mtb extract and capsaicin triggered a significant increase in intracellular [Ca^{2+}] (Figures 2A and 2B).

While Fluo-4 allows for a semiquantitative determination of intracellular [Ca^{2+}], the ratiometric dye Fura-2 allows quantification of intracellular [Ca^{2+}] by determining the ratio of Fura-2 excitation at 340 nm and 380 nM (Grynkiewicz et al., 1985; Iatridou et al., 1994; Kao et al., 2010). Thus, to confirm our results with Fluo-4, we exposed Fura-2-loaded MED17.11 neurons to DMSO, the Mtb extract, and capsaicin and monitored intracellular [Ca^{2+}] over time for individual cells. Each compound was perfused onto the neurons and then removed by washing before the following compound was added (Figure 2C). While DMSO perfusion did not alter intracellular [Ca^{2+}], Mtb extract triggered a rise in intracellular [Ca^{2+}] at ~45 s after exposure as can be seen in individual cell traces (Figure 2C), the average response (Figure 2D), and the quantified response for all cells (Figure 2E). The response of MED17.11 cells to Mtb extract was limited to capsaicin-responsive neurons, as capsaicin non-responsive cells did not demonstrate a significant increase in intracellular [Ca^{2+}] (Figure S1). Furthermore, the Ca^{2+} source was predominantly from intracellular Ca^{2+} stores as there was no difference in the change in intracellular [Ca^{2+}] if MED17.11 neurons were bathed in Ca^{2+}-containing or Ca^{2+}-free media during activation by Mtb extract (Figure S2). To determine whether the specificity of neuronal activation was restricted to the organic compartment, we tested if other Mtb compartments, including cell membrane extracts, cytosol fractions, soluble proteins from the cell wall, Triton X-114 soluble proteins, or secreted proteins can activate MED17.11 neurons. Only the total lipid compartment activated neurons (Table 1).

To determine if the response to the Mtb extract could be observed in primary mouse neurons, we first isolated and cultured murine DRG neurons, loaded them with Fura-2, and exposed them to the Mtb extract. Similar to the MED17.11 cells, primary mouse DRG neurons exposed to the Mtb extract had a large increase in intracellular [Ca^{2+}] at ~45 s after perfusion, in contrast to the DMSO control (Figures 2F–2H), and this response was predominantly in capsaicin-responsive (TRPV1$^+$) neurons (Figure S1). Because the cough reflex is mediated by vagal afferent nerves whose cell bodies are found within the nodose and jugular ganglia (Mazzone and Undem, 2016), we also tested if primary nociceptive neurons isolated from murine nodose and jugular ganglia and loaded with Fura-2 could respond to Mtb extract. As with the primary mouse DRG neurons, exposure of mouse nodose/jugular ganglia neurons to the Mtb extract demonstrated a significant increase in intracellular [Ca^{2+}] entirely in capsaicin-responsive (TRPV1$^+$) cells, in contrast to the DMSO control (Figures 2I–2K and S1). Thus, an organic Mtb extract is sufficient to activate a mouse nociceptive neuronal cell line, primary mouse DRG neurons, and primary mouse nodose/jugular ganglia neurons *in vitro*.

We next assessed if the nociceptive neuron response to the Mtb extract is evolutionarily conserved in humans by measuring the change in intracellular [Ca^{2+}] of primary human DRG neurons obtained from deceased donors (n = 2, one male, one female) after exposure to DMSO, Mtb extract, and capsaicin. Human nociceptive neurons were loaded with fluorescent Fluo-8AM dye and intracellular [Ca^{2+}] measured over time using live cell imaging (Figures 2L–2N). As with the mouse neurons, DMSO-treated human neurons had a minimal response both with respect to intracellular [Ca^{2+}] and number of cells responding. Exposure to Mtb extract generated a substantial increase in intracellular [Ca^{2+}] in multiple cells that were both capsaicin-responsive and non-responsive (Figures 2L–2N and S1). Of the total cell population cultured from the human DRG, 56% in one donor and 100% in another donor of capsaicin-responsive (TRPV1$^+$) neurons were activated by the Mtb extract (Table S1). Thus, an organic Mtb extract activates both mouse and human nociceptive neurons *in vitro*.

Identification of the Nociceptive-Neuron Activating Molecule as Sulfolipid-1

Because we performed all of the preliminary experiments with the Mtb Erdman strain, we next determined the mycobacterial species specificity of the neuron-activating activity of

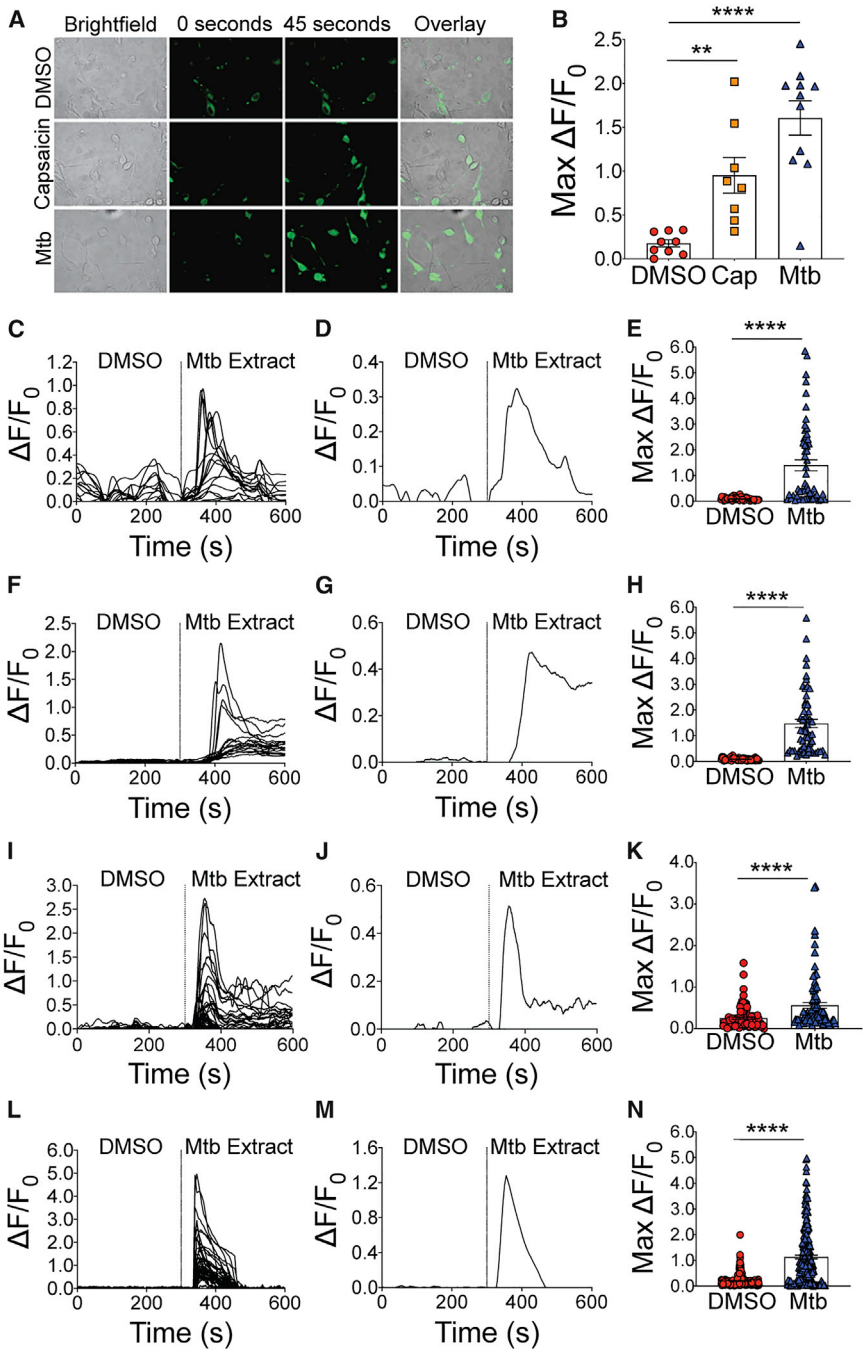

Figure 2. Mtb Extract Increases Intracellular [Ca^{2+}] in Nociceptive Neurons

(A) Bright-field images and images of cells at 488 nm taken at 0 and 45 s after treatment of Fluo-4 loaded MED17.11 cells with DMSO (vehicle), Mtb extract (0.4 mg/mL final), or capsaicin (200 nM).

(B) Quantification of the average max $\Delta F/F_0$ of capsaicin-positive nociceptive neurons after the treatment in A. Error bars are SEM. **p < 0.01, ****p < 0.0001 by Kruskal-Wallace test.

(C–N) Fura-2 (mouse) or Fluo-8AM (human) intracellular calcium assays (Ex 340/380, Em 510 nm) using MED17.11 cells (C–E), primary mouse DRG neurons (F–H), primary mouse nodose/jugular ganglia neurons (I–K), and primary human DRG neurons (L–N). Dashed lines indicate the time when the Mtb extract was added. For each cell type, the $\Delta F/F_0$ trace of representative neurons from a single dish (C, F, I, and L), the average $\Delta F/F_0$ trace for all neurons in a single dish (D, G, J, and M), and the maximum change in $\Delta F/F_0$ fluorescence ratio combining the data from individual neurons in 2 or more experiments (minimum 50 cells) (E, H, K, and N) are shown. For experiments with mouse (MED17.11, DRG, and nodose/jugular) neurons, representative experiments of at least 3 are shown. For human DRG neurons, shown is the combined data from two donors. Error bars in (E), (H), (K), and (N) are SEM. ****p < 0.0001 by paired Student's t test.

mycobacterial organic extracts. We prepared organic extracts from a variety of mycobacterial species including virulent and non-virulent Mtb species, along with non-tuberculous mycobacteria (NTM), and tested their ability to trigger increased intracellular [Ca^{2+}] in MED17.11 neurons. Of the extracts tested, neuronal activation overlapped with virulent bacteria in the Mtb complex (Figure S3; Table 2). We noted that while the virulent Mtb H37Rv strain activated neurons, its attenuated derivative H37Ra (Steenken and Gardner, 1946; Steenken et al., 1934) did not (Table 2). Because H37Ra has a mutation in the PhoP transcription factor that prevents it from producing the cell wall glycolipid SL-1 (Chesne-Seck et al., 2008), we obtained pure SL-1 and tested if it was sufficient to activate MED17.11 cells. Consistent with the lack of SL-1 in the H37Ra strain compared to H37Rv, pure SL-1-activated MED17.11 cells (Figure 3A).

SL-1 is the most abundant sulfated glycolipid located in the outer membrane and cell wall of mycobacteria (Middlebrook et al., 1959), and its presence is unique to pathogenic mycobacteria (Goren et al., 1974). The structure of SL-1 includes a disaccharide trehalose-2-sulfate (T2S) core that is modified with four fatty acyl units (typically 2 hydroxypthioceranic acids, 1 pthiocerenic acid, and 1 palmitic acid) (Layre et al., 2011) (Figure 3B, left). In addition to SL-1, Mtb produces several similarly complex cell wall lipids such as trehalose monomycolate (TMM), trehalose dimycolate (TDM; also known as cord factor), phthiocerol dimycocerosate (PDIM), and others (Figure 3B, center; Table 1). Thus, to assess the chemical specificity of the neuronal response to SL-1, we first determined if the response to SL-1 was saturable by performing a dose response experiment using MED17.11 neurons, yielding an EC_{50} for SL-1

Table 1. Mycobacterial Compartments or Compounds and Ca^{2+} Response

Compound	Triggers Increased $[Ca^{2+}]$
DMSO	–
Capsaicin	+
M. canettii total lipids	+
H37Rv total lipids (normoxic)	+
H37Rv total lipids (hypoxic)	+
CDC1551 cell membrane extract	–
HN878 cell membrane extract	–
H37Rv cell membrane extract	–
CDC1551 cytosol fraction	–
H37Rv cytosol fraction	–
H37Rv soluble cell wall proteins	–
H37Rv TX-114 soluble proteins	–
H37Rv purified lipoarabinomannan (LAM)	–
CDC1551 culture filtrate proteins	–
HN878 culture filtrate proteins	–
Sulfolipid-1	+
Trehalose monomycolate	–
Trehalose dimycolate	–
C24:1 mono-sulfo-galactosyl(β) ceramide (d18:1/24:1)	–
Galactocerebroside	–
H37Rv phosphatidylinositol mannosides 1 & 2 ($PIM_{1,2}$)	–
H37Rv phthiocerol dimycocerosate (PDIM)	–
Trehalose	–
Trehalose-2-sulfate	+

Various mycobacterial compartments including cell wall, lipid and protein mixtures, or isolated compounds were tested for their ability to induce increased $[Ca^{2+}]$ in MED17.11 neurons.

of 33 nM (Figure 3C). We next determined the ability of similarly complex molecules to activate nociceptive neurons by exposing MED17.11 cells to purified Mtb lipids. Of the tested lipids, only SL-1 activated neurons (Figure 3A; Table 1). In addition, only extracts from mycobacterial species that produce complex sulfated glycolipids were able to activate MED17.11 neurons including species of the Mtb complex (producers of SL-1) and *M. avium* (producer of a sulfated glycopeptidolipid but not SL-1) (Mougous et al., 2002a) (Figure S4; Table 2). Although *M. smegmatis* has been reported to produce small sulfated compounds (Mougous et al., 2002b; Rivera-Marrero et al., 2002), it does not produce SL-1 (Mougous et al., 2002b; Rivera-Marrero et al., 2002), and an organic extract from *M. smegmatis* did not activate MED17.11 neurons (Figure S4; Table 2). Finally, mammalian cells including oligodendrocytes and Schwann cells produce a sulfated sphingolipid called sulfatide (3-O-sulfogalactosylceramide) (Figure 3B, right) that comprises 4% of myelin lipids (Takahashi and Suzuki, 2012). To determine if mammalian sulfatide could also activate nociceptive neurons and to further test the chemical specificity of neuronal activation, we exposed MED17.11 neurons to sulfatide and observed that neither sulfatide nor its non-sulfated analog galactocerebroside (Figure 3B) were able to trigger increased intracellular $[Ca^{2+}]$ (Figure 3D). Thus, SL-1 alone can activate neurons and the neuronal response to SL-1 does not represent a generic response to non-sulfated mycobacterial cell wall glycolipids or sulfated monosaccharide lipids.

SL-1 is synthesized in mycobacteria through an enzymatic pathway initiated by sulfation of the symmetric disaccharide trehalose to trehalose-2-sulfate (T2S) by the enzyme sulfotransferase 0 (Stf0), followed by a series of acylation reactions (Figure 3E) (Seeliger et al., 2012). Importantly, genetic deletion of *stf0* in Mtb results in a failure to produce SL-1 (Mougous et al., 2004). To determine if SL-1 synthesis was necessary for neuronal activation, we tested organic extracts from Mtb Erdman wild-type, Mtb Erdman Δ*stf0*, and the complemented strain Mtb Erdman Δ*stf0::stf0* for their ability to activate MED17.11 neurons. While the organic extract from the Mtb Erdman Δ*stf0* strain failed to activate neurons, both the Mtb wild-type and Mtb Erdman Δ*stf0::stf0* extracts triggered neuronal activation (Figure 3F). We also verified that SL-1 was present in the wild-type and Mtb Erdman Δ*stf0::stf0* extracts, but not in the Mtb Erdman Δ*stf0* extract (Figure S5). To confirm that the Mtb Erdman Δ*stf0* extract did not suppress the response of MED17.11 cells to another ligand, we exposed MED17.11 cells first to the Mtb Erdman Δ*stf0* extract followed by pure SL-1 and observed that MED17.11 retained their ability to respond (Figure 3G).

In order to characterize the minimal SL-1 precursor capable of activating nociceptive neurons, we prepared extracts from Mtb mutants at each step of the SL-1 biosynthetic pathway and tested their ability to activate MED17.11 cells. As expected from prior studies (Converse et al., 2003; Kumar et al., 2007; Seeliger et al., 2012), pathway mutants accumulated precursor molecules through mass action (Figure S5). Interestingly, while an extract from the Mtb Erdman Δ*stf0* again failed to activate neurons, extracts from mutants in all subsequent steps retained a modest ability to activate neurons (Figure 3H). Thus, our genetic analysis demonstrated that while SL-1 precursors such as SL-659 and SL-1278 potentially activate neurons, T2S is the minimal molecule capable of neuronal activation in Mtb extracts. To confirm this result, we chemically synthesized T2S (Figure S6) and tested if it could also activate neurons. Consistent with the genetic results (Figure 3H), while the non-sulfated precursor trehalose did not activate neurons, chemically synthesized T2S activated neurons (Figure 3I). Thus, synthesis of SL1 is both necessary and sufficient to activate MED17.11 neurons *in vitro*, and the organically synthesized precursor T2S also activates MED17.11 neurons.

SL-1 Activates Primary Mouse and Human Neurons

We next determined if SL-1 was sufficient to activate primary mouse DRG and nodose/jugular ganglia-derived neurons as well as human DRG neurons. MED17.11 neurons (Figures 4A–4C), primary mouse DRG neurons (Figures 4D–4F), primary mouse nodose/jugular ganglia neurons (Figures 4G–4I), or primary human DRG neurons (Figures 4J–4L; Table S1) were

Table 2. Bacterial Strain Extract, Production of SL-1, and Ca^{2+} Response

Bacterial Strain	Produces SL-1	Triggers Increased [Ca^{2+}]
M. tuberculosis Erdman	+	+
M. tuberculosis HN878	+	+
M. tuberculosis CDC1551	+	+
M. tuberculosis H37Rv	+	+
M. tuberculosis H37Ra	–	–
M. avium	–	+
M. marinum	–	–
M. smegmatis ($mc^2$155)	–	–
M. bovis	–	–
M. canettii	+	+
E. coli (MACH1)	–	–

Extracts from various mycobacterial species were prepared and tested for their ability to induce increased [Ca^{2+}] in MED17.11 neurons. Production of sulfolipid by each bacterial species is also shown.

loaded with Fura-2 (MED17.11 or mouse) or Fluo-8AM (human) and exposed to either DMSO or SL-1. Focusing on only capsaicin responsive, $TRPV1^+$ neurons, individual mouse (Figures 4A, 4C, 4D, 4F, 4G, and 4I) and human (Figures 4J and 4L) neurons displayed a large increase in intracellular [Ca^{2+}] 45 s after exposure to SL-1, similar to our previous observations with the organic Mtb extracts (Figure 2). Both the average response of capsaicin responsive cells (Figures 4B, 4E, 4H, and 4K) and the maximum fluorescence per cell (Figures 4C, 4F, 4I, and 4L) confirmed that SL-1 is a potent agonist of both primary mouse and human capsaicin-responsive, $TRPV1^+$ neurons. The population of capsaicin non-responsive cells did not show a specific response to SL-1 (Figure S1). Thus, SL-1 alone is sufficient to activate both mouse and human nociceptive neurons.

SL-1 Induces Coughing in Naive Guinea Pigs

Having identified SL-1 as an activator of nociceptive neurons in cell culture, we next evaluated if SL-1 could induce cough in unrestrained, naive, healthy guinea pigs. We nebulized extracts from Mtb Erdman wild-type, Mtb ErdmanΔ*stf0* and Mtb ErdmanΔ*stf0::stf0* (20 mg/mL final), or citric acid (0.4 M) into the WBP chambers and monitored cough for 20 min. As before (Figure 1D), individual animals were exposed to each extract or compound on alternating days. Both the Mtb Erdman wild-type and the Mtb ErdmanΔ*stf0::stf0* extracts induced a similar number of coughs as citric acid, while the SL-1-deficient Mtb ErdmanΔ*stf0* extract did not induce coughing (Figure 5A). Furthermore, the response to the Mtb ErdmanΔ*stf0* extract was comparable to the vehicle control (Figure 5A). To determine if SL-1 alone was a nociceptive, cough-inducing molecule, we exposed healthy guinea pigs to nebulized, pure SL-1 (250 μg/mL) and observed a significant cough response (Figure 5B). Thus, the presence of SL-1 synthesis in the Mtb Erdman extract is necessary, and pure SL-1 alone is sufficient to induce cough in healthy guinea pigs.

Genetic Disruption of SL-1 Synthesis Prevents Cough during Mtb Infection of Guinea Pigs

Finally, we tested if the presence of SL-1 during an Mtb infection of guinea pigs would impact the incidence of cough. We infected guinea pigs with Mtb Erdman wild-type, Mtb ErdmanΔ*stf0*, or Mtb ErdmanΔ*stf0::stf0* via low dose aerosol, monitored coughing during the course of infection, and included an uninfected group as a control. At day 0, the lung inocula were similar between the Mtb strains, and at 6 weeks, when the animals were beginning to show signs of disease, there was no difference in lung CFUs (Figure 5C). Likewise, there was no difference between the strains in lung pathology as assessed by histology (Figure 5D) and quantification of percent lung inflammation (Figure 5E). However, at the 6-week time point, we observed an increase in coughing in both the Mtb Erdman wild-type infected and Mtb ErdmanΔ*stf0::stf0* cohorts (Figure 5F). In contrast, except for one outlier animal in the Mtb ErdmanΔ*stf0* cohort, the cough measurements in the Mtb ErdmanΔ*stf0* cohort were comparable to uninfected controls (Figure 5F). Thus, we conclude that the coughing observed in Mtb-infected guinea pigs is due to the synthesis of SL-1.

DISCUSSION

In this study, we determined that both pulmonary Mtb infection and an organic extract from Mtb induce cough in guinea pigs, and an Mtb organic extract activates a neuronal cell line and primary neurons from both mice and humans. Through a combination of intracellular Ca^{2+} imaging assays with mycobacterial extracts and isolated Mtb lipids, we identified SL-1 as the mycobacterial product responsible for neuronal activation. Genetic ablation of SL-1 synthesis in Mtb prevented neuronal activation and cough induction by Mtb extracts, and SL-1 alone was sufficient to induce cough in naive guinea pigs. Finally, guinea pigs infected with Mtb lacking SL-1 synthesis had a blunted cough response despite having a high bacterial burden and pulmonary pathology consistent with active tuberculosis. Together, our data demonstrate a previously undescribed role for Mtb SL-1 in nociceptive neuronal activation and cough induction.

SL-1 was identified as a major component of the Mtb cell wall more than 60 years ago (Middlebrook et al., 1959), but its activity has remained elusive despite the fact that SL-1 represents 1% of the dry weight of Mtb (Goren, 1970a). Because virulence of Mtb strains correlated with the abundance of SL-1 (Goren et al., 1974), it was proposed nearly 5 decades ago that SL-1 is an Mtb virulence factor. However, Mtb mutants that fail to produce SL-1 are not attenuated in mice (Gilmore et al., 2012; Rousseau et al., 2003) or guinea pigs (Rousseau et al., 2003) although SL-1 deficiency enhances Mtb survival within human macrophages potentially through increased resistance to cationic peptides (Gilmore et al., 2012). Our findings are consistent with the *in vivo* evidence that SL-1 is not a classic virulence factor that enhances Mtb survival. Based on our cell culture and *in vivo* data, and the observation that only pathogenic mycobacteria produce SL-1 (this report and reviewed in Daffe et al., 2014; Minnikin et al., 2002), we uncover a heretofore unrecognized function of SL-1 in nociceptive neuron activation and cough induction. Because cough is a major mechanism of Mtb transmission, we propose

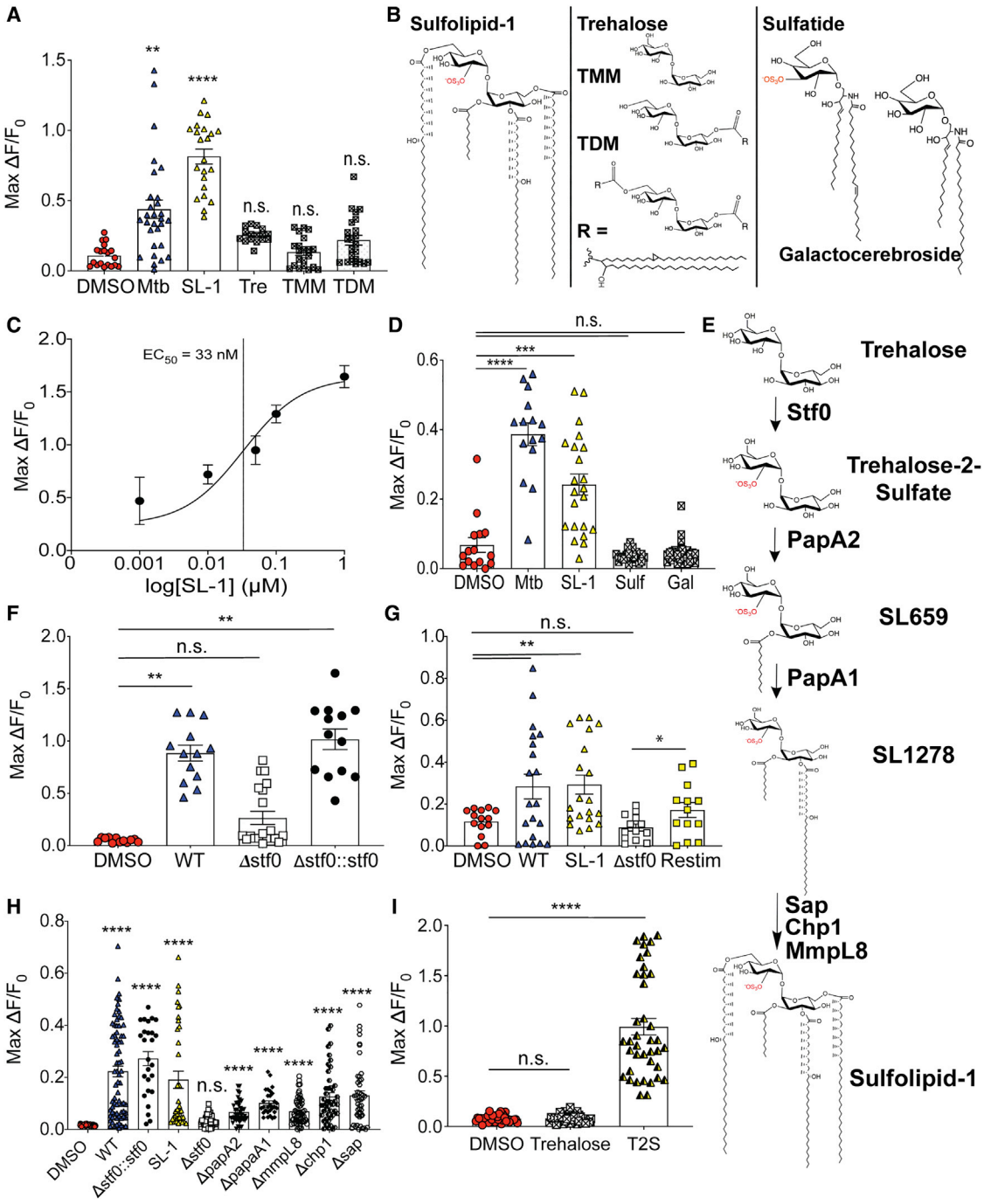

Figure 3. Identification and Characterization of SL-1 as the Nociceptive-Neuron Activating Molecule

(A) Max ΔF of Fluo-4 loaded MED17.11 cells after treatment with DMSO, Mtb Erdman organic extract (Mtb), sulfolipid-1 (SL-1), trehalose (Tre), trehalose monomycolate (TMM), and trehalose dimycolate (TDM).

(B) Structures of SL-1, TMM, TDM, sulfatide, and galactocerebroside.

(C) Dose response of SL-1 using Fura-2 loaded MED17.11 cells. EC_{50} calculated by nonlinear regression analysis.

(D) Max $\Delta F/F_0$ of Fluo-4 loaded MED17.11 cells after treatment with DMSO, Mtb organic extract, SL-1, sulfatide (Sulf) or galactocerebroside (Gal).

(E) Biosynthetic pathway of SL-1. Stf0 (trehalose 2-sulfotransferase; Rv0295c), PapA2 (polyketide synthase-associated protein A2; acyltransferase; Rv3820c), PapA1 (polyketide synthase-associated protein A1; acyltransferase; Rv3824c), Sap (sulfolipid-1-addressing protein; sulfolipid exporter; Rv3821), Chp1 (cutinase-like hydrolase protein; SL1278 acyltransferase; Rv3822), and MmpL8 (sulfolipid-1 exporter, Rv3823c).

(F) Max $\Delta F/F_0$ of Fluo-4 loaded MED17.11 cells after treatment with wild-type Mtb, Mtb*Δstf0* (Δstf0), and Mtb*Δstf0::stf0* complemented (stf0::stf0) extracts.

(legend continued on next page)

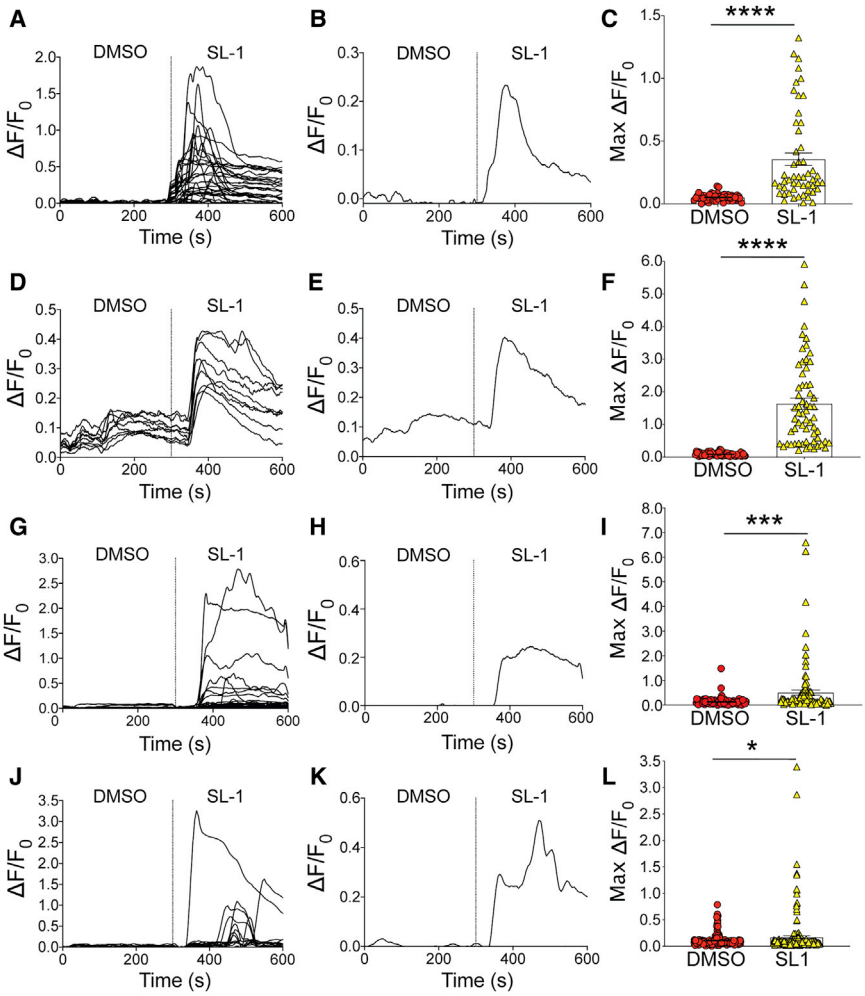

Figure 4. SL-1 Activates Both Mouse and Human DRGs *In Vitro*

(A–C) Intracellular [Ca^{2+}] measurement using MED17.11 cells loaded with Fura-2.

(D–F) Intracellular [Ca^{2+}] measurement using primary mouse DRG neurons loaded with Fura-2.

(G–I) Intracellular [Ca^{2+}] measurement using primary mouse nodose/jugular ganglia neurons loaded with Fura-2.

(J–L) Intracellular [Ca^{2+}] measurement using primary human DRG neurons loaded with Fura-8AM. Dashed lines represent the addition of SL-1. For each, the $\Delta F/F_0$ trace of representative neurons from a single dish (A, D, G, and J), the average $\Delta F/F_0$ trace for all neurons in a single dish (B, E, H, and K), and the maximum change in $\Delta F/F_0$ fluorescence ratio combining the data from individual neurons in 2 or more experiments (minimum 50 cells) (C, F, I, and L) are shown. For experiments with mouse neurons (MED17.11, DRG and nodose/jugular) representative experiments of at least 3 are shown. For human DRG neurons, shown is the combined data from two donors. Error bars in (C), (F), (I), and (L) are SEM. *$p < 0.05$, ***$p < 0.001$, ****$p < 0.0001$ by Student's t test.

that SL-1 is a major contributor to the spread of Mtb from infected to naive individuals.

In addition to Mtb, other mycobacterial species interact with the nervous system through production of complex molecules. For example, *M. ulcerans*, the etiologic agent of Buruli ulcer, causes peripheral anesthesia through the direct activity of a polyketide known as mycolactone (George et al., 1999) on peripheral nerves (Marion et al., 2014). To date, mycolactone has not been isolated from Mtb. Conversely, *M. ulcerans* does not produce SL-1 owing to genomic loss of the pks2 locus (Stinear et al., 2007), suggesting that each species has evolved unique neuromodulatory molecules to facilitate its own lifestyle. Indeed, neuromodulatory molecules have also been observed in gram-negative and gram-positive organisms. Both lipopolysaccharide from *E. coli* (Ochoa-Cortes et al., 2010) and formyl peptides and alpha-hemolysin from *Staphylococcus aureus* (Chiu et al., 2013) activate nociceptive neurons to trigger a pain response and inhibit innate immunity (Baral et al., 2018; Pinho-Ribeiro et al., 2018). Thus, direct neuronal engagement by bacterial molecules to either enhance or suppress cellular responses reflects a common virulence strategy of pathogens.

We tested a variety of Mtb isolates and mycobacterial strains for their ability to produce SL-1 and increase intracellular [Ca^{2+}] in neurons. We observed a direct relationship between the presence of a complex sulfolipid and neuronal activation. Notably, in the matched pair of virulent (H37Rv) and attenuated (H37Ra) strains, SL-1 synthesis is lacking due to a mutation in PhoP (Chesne-Seck et al., 2008), a phenotype that is corroborated in Mtb mutants of the PhoPR two-component system (Gonzalo Asensio et al., 2006; Walters et al., 2006). Likewise, an extract from *M. bovis* did not increase neuronal [Ca^{2+}] and did not have SL-1, in accordance with the observations that *M. bovis*, like H37Ra, is also mutated in the PhoP/PhoR two component system (Gonzalo-Asensio et al., 2014). While children typically develop either cervical lymphadenopathy or gastrointestinal disease when infected with *M. bovis* owing to ingestion of contaminated dairy products (Dankner et al., 1993), primary pulmonary disease occurs in ~50% of adults, in line with probable airborne

(G) Max $\Delta F/F_0$ of Fluo-4 loaded MED17.11 cells after treatment with Mtb extract, pure SL-1, MtbΔ*stf0* (Δstf0), or reactivation of MtbΔ*stf0* extract treated cells by the addition of SL-1. *$p < 0.05$ by paired Student's t test for the MtbΔ*stf0* versus restimulation experiment.

(H) Max $\Delta F/F_0$ of Fluo-4 loaded MED17.11 cells after treatment with extracts from Mtb mutants in the SL-1 synthesis pathway.

(I) Max $\Delta F/F_0$ of Fura-2 loaded MED17.11 cells after treatment with trehalose or synthetic T2S. Experiments are representative of at least 3 replicates. Error bars are SEM. **$p < 0.01$, ***$p < 0.005$, ****$p < 0.0001$ by Kruskal-Wallace (A, D, F, G, H) or Friedman's test (I).

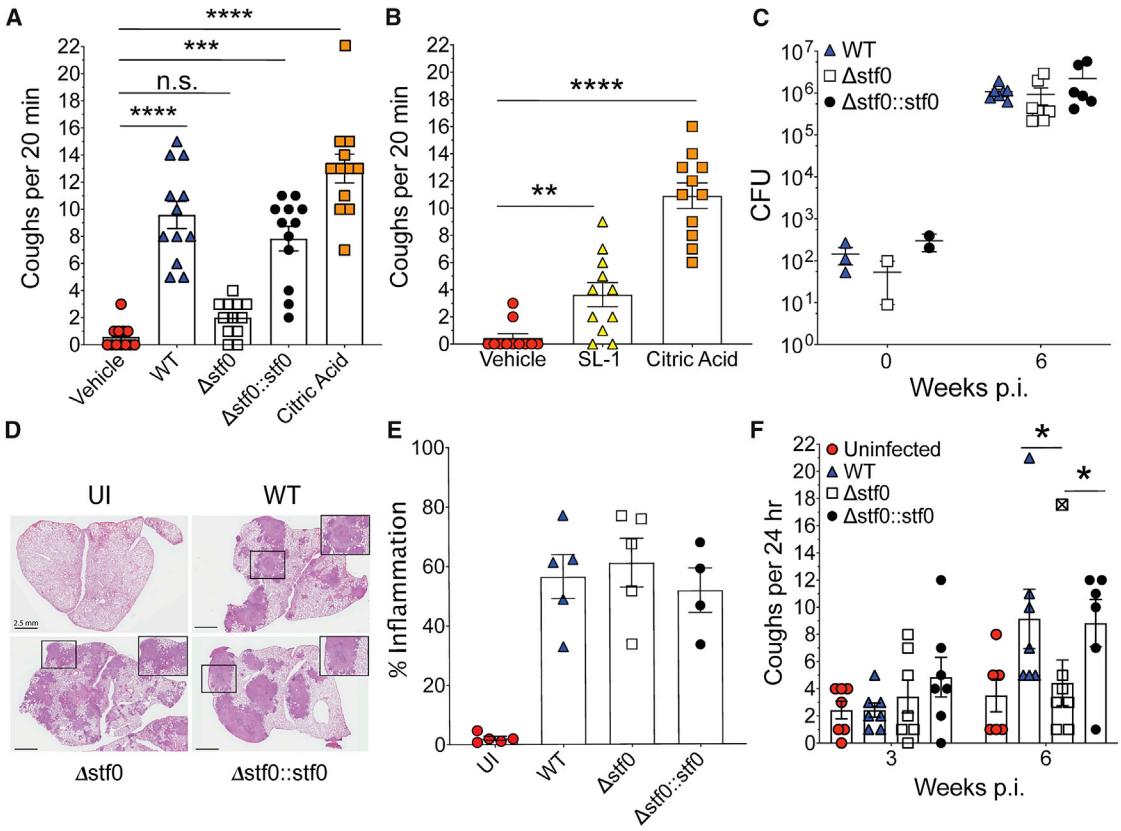

Figure 5. Nebulized SL-1 and SL-1-Producing Mtb Strains Induce Cough

(A) Cough quantification in naive, unrestrained guinea pigs following nebulization of vehicle control (PBS + 10% methanol), wild-type Mtb extract, Mtb*Δstf0* extract (Δstf0), Mtb*Δstf0::stf0* (*Δstf0::stf0*) extract, or citric acid (0.4 M). All extract concentrations were 20 mg/mL.

(B) Cough quantification in naive, unrestrained guinea pigs following nebulization of vehicle control, citric acid (0.4 M), or purified SL-1 (250 μg/mL; estimated max headspace concentration of 12.5 μM). For experiments with Mtb extracts or pure SL-1, data are combined from 2 independent experiments. Error bars are SEM. $^{**}p < 0.01$, $^{***}p < 0.005$, $^{****}p < 0.0001$ by Friedman's test.

(C) Inoculum and week 6 CFU from the right lung of guinea pigs infected with WT Mtb (WT), Mtb*Δstf0* (Δstf0), and Mtb*Δstf0::stf0* (*Δstf0::stf0*).

(D) Histology of left lung from a representative guinea pig from each treatment group at 6 weeks plus an uninfected control (UI). Scale bar, 2.5 mm. Box magnification shows granulomas.

(E) Quantification of (D) showing the percent inflammation from each treatment group (n = 4–5 animals per group). Error bars are SEM.

(F) 24-h guinea pig cough quantification of the number of coughs per guinea pig at 3- and 6-weeks post infection from the wild-type Mtb (WT), Mtb*Δstf0* (Δstf0), and Mtb*Δstf0::stf0* (*Δstf0::stf0*) infected groups and 1 uninfected control group (UI). Each point represents an individual animal. Error bars are SEM. $^{*}p < 0.05$ by Kruskal-Wallis test. Data point identified by outlier analysis indicated with a.

acquisition either from infected livestock or humans (Dankner et al., 1993; Vayr et al., 2018). Because cough is a feature of pulmonary tuberculosis disease caused by *M. bovis* in both livestock and humans, it is likely that molecules other than sulfolipids are involved in *M. bovis*-mediated cough and transmission. In contrast to *M. bovis* and Mtb H37Ra, an organic extract from the NTM species *M. avium* also activated neurons, consistent with its known production of a complex sulfated glycopeptidolipid (Mougous et al., 2002a). Chronic cough is a feature of *M. avium* infection in immunocompromised individuals such as those with human immunodeficiency virus (HIV) (Daley, 2017), cystic fibrosis (Martiniano et al., 2016), and Lady Windermere syndrome (Reich and Johnson, 1992). While the general consensus is that most primary pulmonary NTM infections are due to exposure to environmental reservoirs (Daley and Griffith, 2010; Griffith et al., 2007; Jeon, 2019), there are conflicting data on the possibility of human-to-human transmission of NTM (Bryant et al., 2013, 2016; Doyle et al., 2019). Thus, as with *M. bovis*, *M. avium* induced cough and possible airborne transmission occur in an SL-1 independent manner, although for *M. avium* its sulfated glycopeptidolipid may have an analogous activity.

In addition to Mtb, many viral and bacterial organisms such as measles virus, rhinovirus, coronavirus, influenza virus, *Bordetella pertussis*, and *Mycoplasma pneumonia* have cough as a primary symptom and are transmitted via airborne or droplet particles. In the case of airway viruses, it has been proposed that infections can sensitize cough-evoking sensory nerves through upregulation of receptors involved in cough hypersensitivity (Abdullah et al., 2014; Omar et al., 2017), induction of inflammatory cytokines, leukotrienes, and neuropeptides (Dicpinigaitis, 2014; Footitt and Johnston, 2009), and excess production of airway

mucous (Nadel, 2013). Some infections can also cause cough after pathogen clearance. Such post-infectious cough states are similar to pain responses in other tissues that are mediated by nociceptive sensory neurons such that pain signaling commonly outlasts the presence of the original stimulus (Price and Inyang, 2015; Reichling and Levine, 2009). Thus, post-infectious cough might be similar to a chronic pain state where there is ongoing afferent nociceptive input for weeks or months after the injury has healed. Like viral pathogens, Mtb also induces production of a variety of eicosanoids and leukotrienes such as leukotriene B(4) (Tobin et al., 2010) that can function as an agonist of the TRPV1 cough receptor (Koskela et al., 2012). In addition, extracellular ATP (eATP), a damage-associated molecular pattern (Schmid and Evans, 2019) that can modulate host immunity to Mtb infection (Lammas et al., 1997; Molloy et al., 1994) is a ligand for the purinergic ion channel family (P2X). As the P2X3 receptor has been identified as a cough receptor and possible drug target for chronic cough (Abdulqawi et al., 2015; Bonvini and Belvisi, 2017; Garceau and Chauret, 2019), it is also possible that eATP could activate neuronal P2X3 receptors during Mtb infection. In this study, animals infected with an Mtb strain deficient only in SL-1 synthesis had significantly reduced cough. While we did not measure eicosanoids, leukotrienes or eATP in the lungs of infected animals, overall lung inflammation was equal between wild-type and mutant Mtb infected guinea pigs. Furthermore, our observation that pure SL-1 and wild-type Mtb, but not MtbΔ*stf0*, organic extract rapidly induced cough in naive guinea pigs suggests that the mechanism of cough is through direct activation of a neuronal receptor by SL-1 rather than indirectly through production of a secondary metabolite. Thus, we identify SL-1 as a pathogenic bacterial product with cough-inducing activity.

In this work, we demonstrate that SL-1 is necessary and sufficient for cough induction in guinea pigs. Because guinea pigs and humans demonstrate a similar cough reflex to noxious agonists (Canning, 2008; Laude et al., 1993), SL-1 may also induce cough in humans. Although a link between Mtb virulence and the production of sulfolipids has previously been suggested (Goren et al., 1974), whether SL-1 is required for Mtb transmission remains unknown (Shiloh, 2016). Among the Mtb strains we tested, the HN878 W-Beijing strain is considered to be the most transmissible based on epidemiologic data (Karmakar et al., 2019; Kato-Maeda et al., 2010), and in our hands it produces SL-1 like the virulent laboratory strains Mtb Erdman, CDC1551, and H37Rv. Because our mass spectrometry analysis was qualitative, we are unable to correlate epidemiologic transmission data with SL-1 production. We are currently developing methods to quantify SL-1 in mycobacterial extracts using mass spectrometry as well as methods to safely test Mtb transmission between experimental animals in large scale. Future work will test the impact of SL-1 and cough in the transmission of Mtb as well as the role of putative SL-1 receptors in these processes.

Our results reveal a previously undescribed role for a mycobacterial glycolipid, SL-1, in neuronal activation and cough induction. These findings provide new directions not only in the study of Mtb pathogenesis and transmission, but also a framework for studies on other respiratory pathogens spread by the airborne route. Identification of unique, cough-inducing, pathogen-derived molecules and their host receptors could lead to the development of novel therapeutics that mitigates the spread of disease. For Mtb, in the absence of an effective vaccine to prevent disease acquisition by naive humans, a cough-inhibiting adjuvant therapy has the potential to significantly reduce transmission with major global health implications.

STAR★METHODS

Detailed methods are provided in the online version of this paper and include the following:

- KEY RESOURCES TABLE
- LEAD CONTACT AND MATERIALS AVAILABILITY
- EXPERIMENTAL MODEL AND SUBJECT DETAILS
  - Guinea Pig Studies
  - Mouse Studies
  - Human DRG Studies
  - Bacterial strains and culture conditions
  - Cell lines
- METHOD DETAILS
  - Extraction of mycobacterial lipids
  - Mass spectrometry
  - Mouse DRG neuron isolation and culture
  - Mouse nodose/jugular ganglia neuron isolation and culture
  - Human DRG neuron isolation and culture
  - Live-cell intracellular calcium imaging of MED17.11 neurons and primary mouse DRG and nodose/jugular ganglion neurons
  - Live cell calcium imaging of human DRG neurons
  - Whole-Body Plethysmography
  - Aerosol infection and Guinea Pig Plethysmography
  - Histology
  - Synthesis of trehalose-2-sulfate (T2S)
- QUANTIFICATION AND STATISTICAL ANALYSIS
- DATA AND CODE AVAILABILITY

SUPPLEMENTAL INFORMATION

Supplemental Information can be found online at https://doi.org/10.1016/j.cell.2020.02.026.

ACKNOWLEDGMENTS

We thank B. Levine and members of the Shiloh lab for constructive feedback on the manuscript. We thank G. Dias do Vale and J. McDonald for help with mass spectrometry, C. Bertozzi (Stanford University) for providing Mtb strains, and M. Nassar (University of Sheffield, United Kingdom) for providing MED17.11 cells. We thank BEI Resources, NIAID, NIH, for providing many valuable reagents used in this study as indicated in the STAR Methods. This work is supported by the Burroughs Wellcome Fund (1017894 to M.U.S.), the Welch Foundation (I-1964-20180324 to M.U.S. and I-2010-20190330 to T.Q.), and NIH (R01 NS104200 to G.D.; R01 NS065926 to T.J.P.; U01 AI125939, U19 AI142784, and R21 AI137545 to M.U.S.; 5T32AI005284-40 to H.S.K.; T32AI007520 to C.E.S. and B.L.P.; and T32GM127216 to C.R.D.). T.Q. is supported by the Eugene McDermott Endowed Scholarship, and M.U.S. acknowledges the support of the Disease Oriented Clinical Scholars Program, both at University of Texas Southwestern.

AUTHOR CONTRIBUTIONS

Conceptualization, C.R.R., L.M.K., and M.U.S.; Formal Analysis, C.R.R., B.L.P., L.M.K., C.E.S., and M.U.S.; Funding Acquisition, T.Q., G.D., T.J.P., and M.U.S.; Investigation, C.R.R., B.L.P., H.S.K., L.M.K., C.E.S., L.H.F., M.Z., C.R.D., T.Q., L.G., M.D.B., G.L.M., D.K.N., and M.U.S.; Project Administration, C.R.R. and M.U.S.; Resources, C.H., G.D., and T.J.P.; Supervision, T.Q., G.D., T.J.P., and M.U.S.; Visualization, C.R.R., B.L.P., L.K., and M.U.S.; Writing – Original Draft, C.R.R. and M.U.S.; Writing – Review & Editing, all authors.

DECLARATION OF INTERESTS

The authors declare no competing interests.

Received: October 10, 2019
Revised: January 13, 2020
Accepted: February 10, 2020
Published: March 5, 2020

REFERENCES

Abdullah, H., Heaney, L.G., Cosby, S.L., and McGarvey, L.P. (2014). Rhinovirus upregulates transient receptor potential channels in a human neuronal cell line: implications for respiratory virus-induced cough reflex sensitivity. Thorax *69*, 46–54.

Abdulqawi, R., Dockry, R., Holt, K., Layton, G., McCarthy, B.G., Ford, A.P., and Smith, J.A. (2015). P2X3 receptor antagonist (AF-219) in refractory chronic cough: a randomised, double-blind, placebo-controlled phase 2 study. Lancet *385*, 1198–1205.

Baral, P., Umans, B.D., Li, L., Wallrapp, A., Bist, M., Kirschbaum, T., Wei, Y., Zhou, Y., Kuchroo, V.K., Burkett, P.R., et al. (2018). Nociceptor sensory neurons suppress neutrophil and γδ T cell responses in bacterial lung infections and lethal pneumonia. Nat. Med. *24*, 417–426.

Basaraba, R.J., Dailey, D.D., McFarland, C.T., Shanley, C.A., Smith, E.E., McMurray, D.N., and Orme, I.M. (2006). Lymphadenitis as a major element of disease in the guinea pig model of tuberculosis. Tuberculosis (Edinb.) *86*, 386–394.

Bonvini, S.J., and Belvisi, M.G. (2017). Cough and airway disease: The role of ion channels. Pulm. Pharmacol. Ther. *47*, 21–28.

Brooks, S.M. (2011). Perspective on the human cough reflex. Cough *7*, 10.

Bryant, J.M., Grogono, D.M., Greaves, D., Foweraker, J., Roddick, I., Inns, T., Reacher, M., Haworth, C.S., Curran, M.D., Harris, S.R., et al. (2013). Whole-genome sequencing to identify transmission of Mycobacterium abscessus between patients with cystic fibrosis: a retrospective cohort study. Lancet *381*, 1551–1560.

Bryant, J.M., Grogono, D.M., Rodriguez-Rincon, D., Everall, I., Brown, K.P., Moreno, P., Verma, D., Hill, E., Drijkoningen, J., Gilligan, P., et al. (2016). Emergence and spread of a human-transmissible multidrug-resistant nontuberculous mycobacterium. Science *354*, 751–757.

Burton, M.D., Tillu, D.V., Mazhar, K., Mejia, G.L., Asiedu, M.N., Inyang, K., Hughes, T., Lian, B., Dussor, G., and Price, T.J. (2017). Pharmacological activation of AMPK inhibits incision-evoked mechanical hypersensitivity and the development of hyperalgesic priming in mice. Neuroscience *359*, 119–129.

Canning, B.J. (2007). Encoding of the cough reflex. Pulm. Pharmacol. Ther. *20*, 396–401.

Canning, B.J. (2008). The cough reflex in animals: relevance to human cough research. Hai *186* (*Suppl 1*), S23–S28.

Canning, B.J. (2010). Afferent nerves regulating the cough reflex: mechanisms and mediators of cough in disease. Otolaryngol. Clin. North Am. *43*, 15–25, vii.

Caterina, M.J., Schumacher, M.A., Tominaga, M., Rosen, T.A., Levine, J.D., and Julius, D. (1997). The capsaicin receptor: a heat-activated ion channel in the pain pathway. Nature *389*, 816–824.

Cherry, J.D. (2013). Pertussis: challenges today and for the future. PLoS Pathog. *9*, e1003418.

Chesne-Seck, M.L., Barilone, N., Boudou, F., Gonzalo Asensio, J., Kolattukudy, P.E., Martín, C., Cole, S.T., Gicquel, B., Gopaul, D.N., and Jackson, M. (2008). A point mutation in the two-component regulator PhoP-PhoR accounts for the absence of polyketide-derived acyltrehaloses but not that of phthiocerol dimycocerosates in Mycobacterium tuberculosis H37Ra. J. Bacteriol. *190*, 1329–1334.

Chiu, I.M., Heesters, B.A., Ghasemlou, N., Von Hehn, C.A., Zhao, F., Tran, J., Wainger, B., Strominger, A., Muralidharan, S., Horswill, A.R., et al. (2013). Bacteria activate sensory neurons that modulate pain and inflammation. Nature *501*, 52–57.

Converse, S.E., Mougous, J.D., Leavell, M.D., Leary, J.A., Bertozzi, C.R., and Cox, J.S. (2003). MmpL8 is required for sulfolipid-1 biosynthesis and Mycobacterium tuberculosis virulence. Proc. Natl. Acad. Sci. USA *100*, 6121–6126.

Daffe, M., Crick, D.C., and Jackson, M. (2014). Genetics of Capsular Polysaccharides and Cell Envelope (Glyco)lipids. Microbiol. Spectr. *2*, 14.

Daley, C.L. (2017). Mycobacterium avium Complex Disease. Microbiol. Spectr. *5* https://doi.org/10.1128/microbiolspec.

Daley, C.L., and Griffith, D.E. (2010). Pulmonary non-tuberculous mycobacterial infections. Int. J. Tuberc. Lung Dis. *14*, 665–671.

Dankner, W.M., Waecker, N.J., Essey, M.A., Moser, K., Thompson, M., and Davis, C.E. (1993). Mycobacterium bovis infections in San Diego: a clinicoepidemiologic study of 73 patients and a historical review of a forgotten pathogen. Medicine (Baltimore) *72*, 11–37.

Davidson, S., Copits, B.A., Zhang, J., Page, G., Ghetti, A., and Gereau, R.W. (2014). Human sensory neurons: Membrane properties and sensitization by inflammatory mediators. Pain *155*, 1861–1870.

De Proost, I., Brouns, I., Pintelon, I., Timmermans, J.P., and Adriaensen, D. (2007a). Pulmonary expression of voltage-gated calcium channels: special reference to sensory airway receptors. Histochem. Cell Biol. *128*, 301–316.

De Proost, I., Pintelon, I., Brouns, I., Timmermans, J.P., and Adriaensen, D. (2007b). Selective visualisation of sensory receptors in the smooth muscle layer of ex-vivo airway whole-mounts by styryl pyridinium dyes. Cell Tissue Res. *329*, 421–431.

Dicpinigaitis, P.V. (2014). Effect of viral upper respiratory tract infection on cough reflex sensitivity. J. Thorac. Dis. *6* (*Suppl 7*), S708–S711.

Doran, C., Chetrit, J., Holley, M.C., Grundy, D., and Nassar, M.A. (2015). Mouse DRG Cell Line with Properties of Nociceptors. PLoS ONE *10*, e0128670.

Doyle, R.M., Rubio, M., Dixon, G., Hartley, J., Klein, N., Coll, P., and Harris, K.A. (2019). Cross-transmission is not the source of new Mycobacterium abscessus infections in a multi-centre cohort of cystic fibrosis patients. Clin. Infect. Dis., ciz526.

Fennelly, K.P., Martyny, J.W., Fulton, K.E., Orme, I.M., Cave, D.M., and Heifets, L.B. (2004). Cough-generated aerosols of Mycobacterium tuberculosis: a new method to study infectiousness. Am. J. Respir. Crit. Care Med. *169*, 604–609.

Folch, J., Lees, M., and Sloane Stanley, G.H. (1957). A simple method for the isolation and purification of total lipides from animal tissues. J. Biol. Chem. *226*, 497–509.

Footitt, J., and Johnston, S.L. (2009). Cough and viruses in airways disease: mechanisms. Pulm. Pharmacol. Ther. *22*, 108–113.

Garceau, D., and Chauret, N. (2019). BLU-5937: A selective P2X3 antagonist with potent anti-tussive effect and no taste alteration. Pulm. Pharmacol. Ther. *56*, 56–62.

George, K.M., Barker, L.P., Welty, D.M., and Small, P.L. (1998). Partial purification and characterization of biological effects of a lipid toxin produced by Mycobacterium ulcerans. Infect. Immun. *66*, 587–593.

George, K.M., Chatterjee, D., Gunawardana, G., Welty, D., Hayman, J., Lee, R., and Small, P.L. (1999). Mycolactone: a polyketide toxin from Mycobacterium ulcerans required for virulence. Science *283*, 854–857.

Gilmore, S.A., Schelle, M.W., Holsclaw, C.M., Leigh, C.D., Jain, M., Cox, J.S., Leary, J.A., and Bertozzi, C.R. (2012). Sulfolipid-1 biosynthesis restricts Mycobacterium tuberculosis growth in human macrophages. ACS Chem. Biol. *7*, 863–870.

Glaser, T., Castillo, A.R., Oliveira, Á., and Ulrich, H. (2016). Intracellular Calcium Measurements for Functional Characterization of Neuronal Phenotypes. Methods Mol. Biol. *1341*, 245–255.

Gonzalo Asensio, J., Maia, C., Ferrer, N.L., Barilone, N., Laval, F., Soto, C.Y., Winter, N., Daffé, M., Gicquel, B., Martín, C., and Jackson, M. (2006). The virulence-associated two-component PhoP-PhoR system controls the biosynthesis of polyketide-derived lipids in Mycobacterium tuberculosis. J. Biol. Chem. *281*, 1313–1316.

Gonzalo-Asensio, J., Malaga, W., Pawlik, A., Astarie-Dequeker, C., Passemar, C., Moreau, F., Laval, F., Daffé, M., Martin, C., Brosch, R., and Guilhot, C. (2014). Evolutionary history of tuberculosis shaped by conserved mutations in the PhoPR virulence regulator. Proc. Natl. Acad. Sci. USA *111*, 11491–11496.

Goren, M.B. (1970a). Sulfolipid I of Mycobacterium tuberculosis, strain H37Rv. I. Purification and properties. Biochim. Biophys. Acta *210*, 116–126.

Goren, M.B. (1970b). Sulfolipid I of Mycobacterium tuberculosis, strain H37Rv. II. Structural studies. Biochim. Biophys. Acta *210*, 127–138.

Goren, M.B., Brokl, O., Das, B.C., and Lederer, E. (1971). Sulfolipid I of Mycobacterium tuberculosis, strain H37RV. Nature of the acyl substituents. Biochemistry *10*, 72–81.

Goren, M.B., Brokl, O., and Schaefer, W.B. (1974). Lipids of putative relevance to virulence in Mycobacterium tuberculosis: correlation of virulence with elaboration of sulfatides and strongly acidic lipids. Infect. Immun. *9*, 142–149.

Griffith, D.E., Aksamit, T., Brown-Elliott, B.A., Catanzaro, A., Daley, C., Gordin, F., Holland, S.M., Horsburgh, R., Huitt, G., Iademarco, M.F., et al.; ATS Mycobacterial Diseases Subcommittee; American Thoracic Society; Infectious Disease Society of America (2007). An official ATS/IDSA statement: diagnosis, treatment, and prevention of nontuberculous mycobacterial diseases. Am. J. Respir. Crit. Care Med. *175*, 367–416.

Grynkiewicz, G., Poenie, M., and Tsien, R.Y. (1985). A new generation of Ca2+ indicators with greatly improved fluorescence properties. J. Biol. Chem. *260*, 3440–3450.

Guiard, J., Collmann, A., Gilleron, M., Mori, L., De Libero, G., Prandi, J., and Puzo, G. (2008). Synthesis of diacylated trehalose sulfates: candidates for a tuberculosis vaccine. Angew. Chem. Int. Ed. Engl. *47*, 9734–9738.

Hewlett, E.L., Burns, D.L., Cotter, P.A., Harvill, E.T., Merkel, T.J., Quinn, C.P., and Stibitz, E.S. (2014). Pertussis pathogenesis–what we know and what we don't know. J. Infect. Dis. *209*, 982–985.

Iatridou, H., Foukaraki, E., Kuhn, M.A., Marcus, E.M., Haugland, R.P., and Katerinopoulos, H.E. (1994). The development of a new family of intracellular calcium probes. Cell Calcium *15*, 190–198.

Jankute, M., Cox, J.A., Harrison, J., and Besra, G.S. (2015). Assembly of the Mycobacterial Cell Wall. Annu. Rev. Microbiol. *69*, 405–423.

Jeon, D. (2019). Infection Source and Epidemiology of Nontuberculous Mycobacterial Lung Disease. Tuberc. Respir. Dis. (Seoul) *82*, 94–101.

Jones-López, E.C., White, L.F., Kirenga, B., Mumbowa, F., Ssebidandi, M., Moine, S., Mbabazi, O., Mboowa, G., Ayakaka, I., Kim, S., et al. (2015). Cough Aerosol Cultures of Mycobacterium tuberculosis: Insights on TST / IGRA Discordance and Transmission Dynamics. PLoS ONE *10*, e0138358.

Kao, J.P., Li, G., and Auston, D.A. (2010). Practical aspects of measuring intracellular calcium signals with fluorescent indicators. Methods Cell Biol. *99*, 113–152.

Karmakar, M., Trauer, J.M., Ascher, D.B., and Denholm, J.T. (2019). Hyper transmission of Beijing lineage Mycobacterium tuberculosis: Systematic review and meta-analysis. J. Infect. *79*, 572–581.

Kato-Maeda, M., Kim, E.Y., Flores, L., Jarlsberg, L.G., Osmond, D., and Hopewell, P.C. (2010). Differences among sublineages of the East-Asian lineage of Mycobacterium tuberculosis in genotypic clustering. Int. J. Tuberc. Lung. Dis. *14*, 538–544.

Koch, R. (1912). Gesammelte Werke von Robert Koch. (Leipzig: Verlag von Georg Thieme).

Koskela, H., Purokivi, M., Nieminen, R., and Moilanen, E. (2012). The cough receptor TRPV1 agonists 15(S)-HETE and LTB4 in the cough response to hypertonicity. Inflamm. Allergy Drug Targets *11*, 102–108.

Kumar, P., Schelle, M.W., Jain, M., Lin, F.L., Petzold, C.J., Leavell, M.D., Leary, J.A., Cox, J.S., and Bertozzi, C.R. (2007). PapA1 and PapA2 are acyltransferases essential for the biosynthesis of the Mycobacterium tuberculosis virulence factor sulfolipid-1. Proc. Natl. Acad. Sci. USA *104*, 11221–11226.

Lammas, D.A., Stober, C., Harvey, C.J., Kendrick, N., Panchalingam, S., and Kumararatne, D.S. (1997). ATP-induced killing of mycobacteria by human macrophages is mediated by purinergic P2Z(P2X7) receptors. Immunity *7*, 433–444.

Laude, E.A., Higgins, K.S., and Morice, A.H. (1993). A comparative study of the effects of citric acid, capsaicin and resiniferatoxin on the cough challenge in guinea-pig and man. Pulm. Pharmacol. *6*, 171–175.

Layre, E., Paepe, D.C., Larrouy-Maumus, G., Vaubourgeix, J., Mundayoor, S., Lindner, B., Puzo, G., and Gilleron, M. (2011). Deciphering sulfoglycolipids of Mycobacterium tuberculosis. J. Lipid Res. *52*, 1098–1110.

Lomask, J., and Larson, R.A., (2004). Cough/sneeze analyzer and method. US patent 7104962, filed June 18, 2004 and granted September 12, 2006.

Lurie, M.B. (1930a). Experimental Epidemiology of Tuberculosis: Air-Borne Contagion of Tuberculosis in an Animal Room. J. Exp. Med. *51*, 743–751.

Lurie, M.B. (1930b). Experimental Epidemiology of Tuberculosis: The Effect of Crowding Upon Tuberculosis in Guinea Pigs, Acquired by Contact and by Inoculation. J. Exp. Med. *51*, 729–741.

Lurie, M.B. (1930c). Experimental Epidemiology of Tuberculosis: The Effect of Eliminating Exposure to Enteric Infection on the Incidence and Course of Tuberculosis Acquired by Normal Guinea Pigs Confined with Tuberculous Cage Mates. J. Exp. Med. *51*, 753–768.

Lurie, M.B. (1930d). Experimental Epidemiology of Tuberculosis: The Route of Infection in Naturally Acquired Tuberculosis of the Guinea Pig. J. Exp. Med. *51*, 769–776.

Marion, E., Song, O.R., Christophe, T., Babonneau, J., Fenistein, D., Eyer, J., Letournel, F., Henrion, D., Clere, N., Paille, V., et al. (2014). Mycobacterial toxin induces analgesia in buruli ulcer by targeting the angiotensin pathways. Cell *157*, 1565–1576.

Martiniano, S.L., Nick, J.A., and Daley, C.L. (2016). Nontuberculous Mycobacterial Infections in Cystic Fibrosis. Clin. Chest Med. *37*, 83–96.

Mazzone, S.B. (2005). An overview of the sensory receptors regulating cough. Cough *1*, 2.

Mazzone, S.B., and Undem, B.J. (2016). Vagal Afferent Innervation of the Airways in Health and Disease. Physiol. Rev. *96*, 975–1024.

Middlebrook, G., Coleman, C.M., and Schaefer, W.B. (1959). Sulfolipid from Virulent Tubercle Bacilli. Proc. Natl. Acad. Sci. USA *45*, 1801–1804.

Minnikin, D.E., Kremer, L., Dover, L.G., and Besra, G.S. (2002). The methyl-branched fortifications of Mycobacterium tuberculosis. Chem. Biol. *9*, 545–553.

Molloy, A., Laochumroonvorapong, P., and Kaplan, G. (1994). Apoptosis, but not necrosis, of infected monocytes is coupled with killing of intracellular bacillus Calmette-Guérin. J. Exp. Med. *180*, 1499–1509.

Morice, A.H., Fontana, G.A., Belvisi, M.G., Birring, S.S., Chung, K.F., Dicpinigaitis, P.V., Kastelik, J.A., McGarvey, L.P., Smith, J.A., Tatar, M., and Widdicombe, J.; European Respiratory Society (ERS) (2007). ERS guidelines on the assessment of cough. Eur. Respir. J. *29*, 1256–1276.

Mougous, J.D., Green, R.E., Williams, S.J., Brenner, S.E., and Bertozzi, C.R. (2002a). Sulfotransferases and sulfatases in mycobacteria. Chem. Biol. *9*, 767–776.

Mougous, J.D., Leavell, M.D., Senaratne, R.H., Leigh, C.D., Williams, S.J., Riley, L.W., Leary, J.A., and Bertozzi, C.R. (2002b). Discovery of sulfated metabolites in mycobacteria with a genetic and mass spectrometric approach. Proc. Natl. Acad. Sci. USA *99*, 17037–17042.

Mougous, J.D., Petzold, C.J., Senaratne, R.H., Lee, D.H., Akey, D.L., Lin, F.L., Munchel, S.E., Pratt, M.R., Riley, L.W., Leary, J.A., et al. (2004). Identification, function and structure of the mycobacterial sulfotransferase that initiates sulfolipid-1 biosynthesis. Nat. Struct. Mol. Biol. *11*, 721–729.

Nadel, J.A. (2013). Mucous hypersecretion and relationship to cough. Pulm. Pharmacol. Ther. *26*, 510–513.

Ochoa-Cortes, F., Ramos-Lomas, T., Miranda-Morales, M., Spreadbury, I., Ibeakanma, C., Barajas-Lopez, C., and Vanner, S. (2010). Bacterial cell products signal to mouse colonic nociceptive dorsal root ganglia neurons. Am. J. Physiol. Gastrointest. Liver Physiol. *299*, G723–G732.

Omar, S., Clarke, R., Abdullah, H., Brady, C., Corry, J., Winter, H., Touzelet, O., Power, U.F., Lundy, F., McGarvey, L.P., and Cosby, S.L. (2017). Respiratory virus infection up-regulates TRPV1, TRPA1 and ASICS3 receptors on airway cells. PLoS ONE *12*, e0171681.

Orme, I.M., and Ordway, D.J. (2016). Mouse and Guinea Pig Models of Tuberculosis. Microbiol. Spectr. *4* https://doi.org/10.1128/microbiolspec.

Perla, D. (1927). Experimental Epidemiology of Tuberculosis. J. Exp. Med. *45*, 209–226.

Pinho-Ribeiro, F.A., Baddal, B., Haarsma, R., O'Seaghdha, M., Yang, N.J., Blake, K.J., Portley, M., Verri, W.A., Dale, J.B., Wessels, M.R., et al. (2018). Blocking Neuronal Signaling to Immune Cells Treats Streptococcal Invasive Infection. Cell *173*, 1083–1097.

Pintelon, I., Brouns, I., De Proost, I., Van Meir, F., Timmermans, J.P., and Adriaensen, D. (2007). Sensory receptors in the visceral pleura: neurochemical coding and live staining in whole mounts. Am. J. Respir. Cell Mol. Biol. *36*, 541–551.

Price, T.J., and Inyang, K.E. (2015). Commonalities between pain and memory mechanisms and their meaning for understanding chronic pain. Prog. Mol. Biol. Transl. Sci. *131*, 409–434.

Reich, J.M., and Johnson, R.E. (1992). Mycobacterium avium complex pulmonary disease presenting as an isolated lingular or middle lobe pattern. The Lady Windermere syndrome. Chest *101*, 1605–1609.

Reichling, D.B., and Levine, J.D. (2009). Critical role of nociceptor plasticity in chronic pain. Trends Neurosci. *32*, 611–618.

Rivera-Marrero, C.A., Ritzenthaler, J.D., Newburn, S.A., Roman, J., and Cummings, R.D. (2002). Molecular cloning and expression of a novel glycolipid sulfotransferase in Mycobacterium tuberculosis. Microbiology *148*, 783–792.

Rousseau, C., Turner, O.C., Rush, E., Bordat, Y., Sirakova, T.D., Kolattukudy, P.E., Ritter, S., Orme, I.M., Gicquel, B., and Jackson, M. (2003). Sulfolipid deficiency does not affect the virulence of Mycobacterium tuberculosis H37Rv in mice and guinea pigs. Infect. Immun. *71*, 4684–4690.

Schelle, M.W., and Bertozzi, C.R. (2006). Sulfate metabolism in mycobacteria. ChemBioChem *7*, 1516–1524.

Schmid, R., and Evans, R.J. (2019). ATP-Gated P2X Receptor Channels: Molecular Insights into Functional Roles. Annu. Rev. Physiol. *81*, 43–62.

Schneider, C.A., Rasband, W.S., and Eliceiri, K.W. (2012). NIH Image to ImageJ: 25 years of image analysis. Nat. Methods *9*, 671–675.

Seeliger, J.C., Holsclaw, C.M., Schelle, M.W., Botyanszki, Z., Gilmore, S.A., Tully, S.E., Niederweis, M., Cravatt, B.F., Leary, J.A., and Bertozzi, C.R. (2012). Elucidation and chemical modulation of sulfolipid-1 biosynthesis in Mycobacterium tuberculosis. J. Biol. Chem. *287*, 7990–8000.

Shiloh, M.U. (2016). Mechanisms of mycobacterial transmission: how does Mycobacterium tuberculosis enter and escape from the human host. Future Microbiol. *11*, 1503–1506.

Steenken, W., Jr., and Gardner, L.U. (1946). History of H37 strain of tubercle bacillus. Am. Rev. Tuberc. *54*, 62–66.

Steenken, W., Oatway, W.H., and Petroff, S.A. (1934). Biological Studies of the Tubercle Bacillus: Iii. Dissociation and Pathogenicity of the R and S Variants of the Human Tubercle Bacillus (H(37)). J. Exp. Med. *60*, 515–540.

Stinear, T.P., Seemann, T., Pidot, S., Frigui, W., Reysset, G., Garnier, T., Meurice, G., Simon, D., Bouchier, C., Ma, L., et al. (2007). Reductive evolution and niche adaptation inferred from the genome of Mycobacterium ulcerans, the causative agent of Buruli ulcer. Genome Res. *17*, 192–200.

Takahashi, T., and Suzuki, T. (2012). Role of sulfatide in normal and pathological cells and tissues. J. Lipid Res. *53*, 1437–1450.

Tanaka, M., and Maruyama, K. (2005). Mechanisms of capsaicin- and citric-acid-induced cough reflexes in guinea pigs. J. Pharmacol. Sci. *99*, 77–82.

Tobin, D.M., Vary, J.C., Jr., Ray, J.P., Walsh, G.S., Dunstan, S.J., Bang, N.D., Hagge, D.A., Khadge, S., King, M.C., Hawn, T.R., et al. (2010). The lta4h locus modulates susceptibility to mycobacterial infection in zebrafish and humans. Cell *140*, 717–730.

Turner, R.D. (2019). Cough in pulmonary tuberculosis: Existing knowledge and general insights. Pulm. Pharmacol. Ther. *55*, 89–94.

Turner, O.C., Basaraba, R.J., and Orme, I.M. (2003). Immunopathogenesis of pulmonary granulomas in the guinea pig after infection with Mycobacterium tuberculosis. Infect. Immun. *71*, 864–871.

Turner, R.D., and Bothamley, G.H. (2015). Cough and the transmission of tuberculosis. J. Infect. Dis. *211*, 1367–1372.

Vayr, F., Martin-Blondel, G., Savall, F., Soulat, J.M., Deffontaines, G., and Herin, F. (2018). Occupational exposure to human Mycobacterium bovis infection: A systematic review. PLoS Negl. Trop. Dis. *12*, e0006208.

Walters, S.B., Dubnau, E., Kolesnikova, I., Laval, F., Daffe, M., and Smith, I. (2006). The Mycobacterium tuberculosis PhoPR two-component system regulates genes essential for virulence and complex lipid biosynthesis. Mol. Microbiol. *60*, 312–330.

Zaccone, E.J., Lieu, T., Muroi, Y., Potenzieri, C., Undem, B.E., Gao, P., Han, L., Canning, B.J., and Undem, B.J. (2016). Parainfluenza 3-Induced Cough Hypersensitivity in the Guinea Pig Airways. PLoS ONE *11*, e0155526.

STAR★METHODS

KEY RESOURCES TABLE

REAGENT or RESOURCE	SOURCE	IDENTIFIER
Bacterial and Virus Strains		
M. tuberculosis Erdman	Laboratory of J. Cox (UC Berkeley)	N/A
M. tuberculosis HN878	BEI Resources	NR-13647
M. tuberculosis CDC1551	BEI Resources	NR-13649
M. tuberculosis H37Rv	BEI Resources	NR-13648
M. tuberculosis H37Ra	BEI Resources	NR-122
M. tuberculosis Erdman⊿stf0	Laboratory of C. Bertozzi (Stanford)	https://doi.org/10.1038/nsmb802
M. tuberculosis Erdman⊿stf0::stf0	Laboratory of C. Bertozzi (Stanford)	https://doi.org/10.1038/nsmb802
M. tuberculosis Erdman⊿papA1	Laboratory of C. Bertozzi (Stanford)	https://doi.org/10.1073/pnas.0611649104
M. tuberculosis Erdman⊿papA2	Laboratory of C. Bertozzi (Stanford)	https://doi.org/10.1073/pnas.0611649104
M. tuberculosis Erdman⊿mmpl8	Laboratory of C. Bertozzi (Stanford)	https://doi.org/10.1073/pnas.1030024100
M. tuberculosis Erdman⊿chp1	Laboratory of C. Bertozzi (Stanford)	https://doi.org/10.1074/jbc.M111.315473
M. tuberculosis Erdman⊿sap	Laboratory of C. Bertozzi (Stanford)	https://doi.org/10.1074/jbc.M111.315473
M. bovis Karlson and Lessel	ATCC	ATCC 19210
M. avium	BEI Resources	NR-49092
M. marinum	Laboratory of J. Cox (UC Berkeley)	N/A
M. smegmatis mc^2155	Laboratory of J. Cox (UC Berkeley)	N/A
E. coli (MACH1)	Thermo Fisher	Cat#C862003
Biological Samples		
Human: Primary Human DRG neurons	Anabios	https://anabios.com
Chemicals, Peptides, and Recombinant Proteins		
DMSO	Fisher	Cat#BP231-100
Trehalose	Sigma	Cat#T9531
Galactocerebrosides	Sigma	Cat#C4905
C24:1 Mono-Sulfo-Galactosyl(β) Ceramide (d18:1/24:1)	Avanti Polar Lipids	Cat#860571
Capsaicin	Sigma	Cat#M2028
Trehalose-2-Sulfate	This paper	N/A
Sulfolipid-1	BEI Resources	NR-14845
H37Rv PIMs	BEI Resources	NR-14846
H37Rv PDIM	BEI Resources	NR-20328
H37Rv Cell Membrane Extract	BEI Resources	NR-14831
CDC1551 Cell Membrane Extract	BEI Resources	NR-14832
HN878 Cell Membrane Extract	BEI Resources	NR-14833
Trehalose Monomycolate	BEI Resources	NR-48784
Trehalose Dimycolate	BEI Resources	NR-14844
M. canettii total lipids	BEI Resources	NR-40334
H37Rv Normoxic and Hypoxic Total Lipids Kit	BEI Resources	NR-48697
CDC1551 Cytosol Fraction	BEI Resources	NR-14835
H37Rv Cytosol Fraction	BEI Resources	NR-14834
H37Rv Soluble Cell Wall Proteins	BEI Resources	NR-14840
H37Rv TX-114 Soluble Proteins	BEI Resources	NR-14841
H37Rv Purified Lipoarabinomannan (LAM)	BEI Resources	NR-14848
CDC1551 Culture Filtrate Proteins	BEI Resources	NR-14826
HN878 Culture Filtrate Proteins	BEI Resources	NR-14825

(*Continued on next page*)

Continued

REAGENT or RESOURCE	SOURCE	IDENTIFIER
Critical Commercial Assays		
Primary Human DRG Calcium Assay	Anabios	https://anabios.com
Experimental Models: Cell Lines		
Mouse: MED17.11 neuronal cells	Laboratory of M. Nassar (University of Sheffield)	RRID:CVCL_4Y33; https://doi.org/10.1371/journal.pone.0128670
Experimental Models: Organisms/Strains		
Guinea Pig: Male Hartley	Charles River	Crl:HA
Mouse: Male, Institute for Cancer Research (ICR)	Envigo	Hsd:ICR (CD-1)
Human: Primary Human DRG neurons	Anabios	https://anabios.com
Software and Algorithms		
Buxco FinePointe Software	Data Sciences International	https://www.datasci.com/products/software/finepointe-software
MetaMorph Software	Molecular Devices	https://www.moleculardevices.com
MetaFluor Fluorescence Ratio imaging software	Molecular Devices	https://www.moleculardevices.com
ImageJ	Schneider et al., 2012	https://imagej.nih.gov/ij/
Volocity Imaging Software	Perkin Elmer	https://www.perkinelmer.com
Prism 8.0	GraphPad	https://www.graphpad.com

LEAD CONTACT AND MATERIALS AVAILABILITY

Please direct requests for resources and reagents to Lead Contact, Michael Shiloh (Michael.Shiloh@utsouthwestern.edu). Distribution of T2S will require signing a Material Transfer Agreement (MTA) in accordance with the policies of the University of Texas Southwestern Medical Center.

EXPERIMENTAL MODEL AND SUBJECT DETAILS

Guinea Pig Studies

Male Hartley outbred guinea pigs aged 4-6 weeks (weight 200-250 g) were purchased from Charles River Laboratories. Guinea pig health status was monitored daily. For cough studies with Mtb extracts or compounds, animals were naive at the outset of the study. Each experimental animal was treated with vehicle control and extract or compound separated by a day to avoid tachyphylaxis. Guinea pigs were housed in standard cages with Alpha-dri bedding (Shepherd Specialty Papers, Kalamazoo, MI) and provided food and water *ad libitum*. Autoclaved pressed timothy hay cubes (Bioserv, Flemington, NJ) were also provided. Guinea pig experiments were reviewed and approved by the Institutional Animal Care and Use Committee at the University of Texas Southwestern (protocol 2018-102280-USDA) and followed the eighth edition of the Guide for the Care and Use of Laboratory Animals. The University of Texas Southwestern is accredited by the American Association for Accreditation of Laboratory Animal Care (AAALAC).

Mouse Studies

Institute for Cancer Research (ICR) outbred mice originally purchased from Envigo were bred at the University of Texas at Dallas and used for DRG or nodose/jugular ganglion neuron preparation at 4 weeks of age (weight 18-20 g). Mice were housed in standard cages with aspen wood bedding (Lab Supply, Fort Worth, TX) placed on ventilated rack systems with food and water *ad libitum*. Cotton squares were also provided for nesting. Mouse experiments were reviewed and approved by the Institutional Animal Care and Use Committee at the University of Texas at Dallas (protocol #14-04) and followed the eighth edition of the Guide for the Care and Use of Laboratory Animals.

Human DRG Studies

Primary human nociceptive neurons were isolated from DRGs obtained from two anonymous donors. Donor 1 was a 33-year-old female and Donor 2 was a 20-year-old male. All human DRGs used for this study were obtained from brain-dead organ donors in the United States after obtaining informed consent in accordance to Federal and State regulations, and United Network for Organ Sharing (UNOS) policies (Anabios, San Diego, CA).

Bacterial strains and culture conditions

M. tuberculosis Erdman was the predominant lab strain used in the study. Wild-type and mutant strains of *M. tuberculosis* were grown in Middlebrook 7H9 medium or on Middlebrook 7H11 plates supplemented with 10% oleic acid-albumin-dextrose-catalase. Freshly prepared tween 80 (Fisher T164-500) was added to liquid medium to a final concentration of 0.05%. All other mycobacterial species (Table 2, Bacterial strains and Key Resources Table) were grown under similar conditions.

Cell lines

MED17.11 cells (Doran et al., 2015) were provided by M. Nassar and were grown using DMEM F12/Glutamax (Thermo) with pen/strep/glutamine (100 I.U./mL penicillin, 100 μg/mL streptomycin, 292 μg/mL L-glutamine, Corning), 50 units/mL interferon gamma (R&D Systems), 0.5% chick embryonic extract (US Biological). The MED17.11 cell line was not authenticated as mouse short tandem repeat testing was not available at the time the studies were performed. Undifferentiated cells were maintained at 33°C and 5% CO_2 in a humidified incubator. For differentiation and microscopy, 5×10^4 cells were plated onto 35 mm dishes (MatTek) and supplied with differentiation media consisting of DMEM/F12, pen/strep/glutamine, 10% FBS, 10 ng/mL β-FGF (R&D Systems), 0.5 mM di-butyrl cAMP (Sigma), 25 μM forskolin (R&D Systems), 5 μg/mL rock inhibitor Y-27632 (R&D Systems), 100 ng/mL NGF (R&D Systems) and 20 ng/mL GDNF (Sigma). Cells were then maintained at 37°C and 5% CO_2 in a humidified incubator for 7 days, changing the media every 2-3 days.

METHOD DETAILS

Extraction of mycobacterial lipids

Mycobacteria were grown to an OD_{600} of 0.8 in Middlebrook 7H9 supplemented with 0.01% Tween 80. Then, 200 mL of bacteria were collected by centrifugation at 3500 RPM (Allegra X-14R) for 10 min, resuspended in 2 ml of PBS, and transferred to a glass tube containing 45 ml chloroform-methanol (2:1, vol/vol), and placed in a 58°C water bath for 16 hr. Samples were centrifuged at 2000 RPM (Allegra X-14R) for 5 min, and the upper-phase and cell debris was removed. The remaining organic phase was washed with 8 mL of water followed by a final wash with 2 mL methanol-water (1:1, vol/vol) to remove any remaining polar components. Extracts were then dried down using a RotoVap (IKA HB10) or under nitrogen.

Mass spectrometry

Extracts from mycobacteria were first dried down. Dried extracts were then resuspended in 1:1 MeOH:IPA 16 mM NH_4F at a 4 mg/mL final concentration. Samples were manually infused with a syringe on a quadrupole TOF TripleTOF 6600+ mass spectrometer (SCIEX, Framingham, MA). Electrospray ionization source parameters were as follows: ion source gas 1 (GS1) and gas 2 (GS2) set to 25 and 55 psi, respectively; curtain (Cur) gas set to 25 psi; source temperature of 300°C; and ion-spray voltage of −4,500 V in the negative ionization mode. GS1 and GS2 were zero-grade air, while Cur gas was nitrogen. TOF scans from 100-3000 m/z were collected over 60 s with a flow rate of 10 μL/min. Data were analyzed in PeakView (SCIEX) to identify SL_{659} at 659-661 m/z, SL_{1278} at 1277-1279 m/z, and SL-1 at 2000-3000 m/z.

Mouse DRG neuron isolation and culture

Primary mouse DRGs from male ICR mice were extracted, digested and cultured following an established protocol (Burton et al., 2017). Briefly, once dissected, DRGs were placed on ice in Hank's Balanced Salt Solution (HBSS) (Invitrogen). Ganglia were enzymatically dissociated by serial addition of collagenase A (1 mg/ml, Roche Diagnostics, Basel, Switzerland), collagenase D (1 mg/ml; Roche Diagnostics, Basel, Switzerland) and papain (30 μg/ml; Roche Diagnostics, Basel, Switzerland) at 37°C in HBSS, followed by addition of a trypsin inhibitor (1 mg/ml; Roche) that contained bovine serum albumin (bovine serum albumin, 1 mg/ml; Fisher), and the ganglia were further mixed with a polished Pasteur pipette. Disaggregated tissue was then filtered through a 70-μm nylon cell strainer (Falcon; Corning, NY) and resuspended in Dulbecco's modified Eagle's medium F-12 GlutaMax media (Invitrogen) containing 10% fetal bovine serum (Hyclone Laboratories, Inc., South Logan, UT) and 1 × penicillin streptomycin (Invitrogen). The media also contained nerve growth factor (10 ng/ml; Millipore, Billerica, MA) and 5-fluoro-2′-deoxyuridine + uridine (3.0 μg/ml + 7.0 μg/ml; Sigma) to reduce proliferation of glia and fibroblasts. Neurons were cultured on 35 mm dishes (MatTek) coated with poly-D-lysine at 37°C with 95% air and 5% CO_2 for 3-5 days. All DRGs from 4-6 mice were combined to generate approximately 4-6 dishes of primary cells per experiment.

Mouse nodose/jugular ganglia neuron isolation and culture

Primary mouse nodose/jugular ganglia from male ICR mice were extracted, digested and cultured following an established protocol similar to the DRG neuron isolation with slight modifications (Burton et al., 2017). Both sides of the nodose/jugular ganglia from 8-9 mice were combined to generate 2 dishes of primary cells. Neurons were cultured on 35 mm dishes (MatTek) coated with poly-D-lysine (Sigma) and laminin (Sigma) at 37°C with 95% air and 5% CO_2 overnight.

Human DRG neuron isolation and culture

DRGs from 2 human donors from the first thoracic vertebra (T1) through the first sacral vertebra (S1) were used in the present study. The DRGs were stripped of connective tissue and enzymatically digested at 37°C for 2 hr using the methods described by Davidson et al. (2014). Dissociated cells were seeded on 96-well plastic bottom plates (Corning) that had been pre-coated with poly-D-lysine. Cells were maintained in culture at 37°C with 5% CO2 in DMEM/F12 supplemented with 10% horse serum (Thermo Fisher Scientific), 2 mM glutamine, 10 ng/mL hNGF (Cell Signaling Technology), 10 ng/mL GDNF (Peprotech), and penicillin/streptomycin (Thermo Fisher Scientific). Half of the culture media was replaced with fresh media every 3 days.

Live-cell intracellular calcium imaging of MED17.11 neurons and primary mouse DRG and nodose/jugular ganglion neurons

Cells on 35 mm dishes (MatTek) were loaded with Fluo-4 (Thermo, F10471) or Fura-2 (Thermo, F1221). The dye was removed and 1 mL of HBSS with 20 mM HEPES, pH 7.4 (Thermo, 14170112) was added to each dish for 10 min prior to microscopy. A brightfield image was taken prior to cell stimulation and imaging. Fluo-4 microscopy was performed using Spinning Disk Confocal microscopy at 40X (PerkinElmer) with Volocity imaging software (Perkin Elmer). Cells were imaged at 488 nm. After a 10 s baseline recording, cells were treated with controls or extracts for 90 s and images were obtained every 1 s. A waiting period of 2-5 min was performed between treatment of cells with another molecule to minimize neurons being desensitized.

For Fura-2 experiments, after dye loading, cells were placed in 1 mL of HBSS with 20 mM HEPES for 10 minutes prior to recording. Using an Olympus IX73 inverted microscope, data was acquired with MetaFluor Flourescence Ratio imaging software (Olympus) at excitation wavelengths of 340/380 nm and emission wavelength of 510 nm with image acquisition every 1 s. A 100 s baseline was first recorded after which DMSO was added and recording was obtained for 300 s. Next, compounds or extracts were added with continuous recording for 300 s. Finally, 200 nM was capsaicin added with continuous recording for 300 s.

Live cell calcium imaging of human DRG neurons

Experiments were conducted on isolated human DRG neurons from post-mortem donors by Anabios, Inc., San Diego, CA. Cells were loaded with 3 μM Fluo-8-AM (AAT Bioquest) containing 0.1% Pluronic F-127 (Sigma) for 30 min at room temperature. Extracellular solution contained in (mM): 145 NaCl, 3 KCl, 2 $CaCl_2$, 1 $MgCl_2$, 10 HEPES, 10 glucose adjusted to pH 7.4 with NaOH. Fluo-8-loaded cells were excited at 480 nm and emission was collected at 520 nm with a pcoEDGE sCMOS camera (PCO) mounted on an inverted microscope (Olympus IX71). Images were acquired at 0.2 Hz for 5 min, adding the compound of interest or the vehicle (1% DMSO) after 30 s for a total of 2 min, then washing with the external solution. At the end of the response profiling, an additional application of 200 nM capsaicin (Sigma) was performed to identify the nociceptor human DRG neurons. Image acquisition and data analysis were performed using MetaMorph software (Molecular Devices).

Whole-Body Plethysmography

Guinea pigs were placed inside a specialized chamber (Data Sciences International) fitted with a sensitive pressure transducer and an opening for a nebulization device to aerosolize compounds into the chamber. Using the Buxco FinePointe software, the primary cough data recorded were the Bias Flow of the system, the slope of the Bias flow, and the Delta Half Peak Crossing (DHPC) which is the time it takes to transition from the compression phase to the expulsive phase during respiration (Lomask and Larson, 2004). While not used in the cough analysis, other respiratory data, such as respiration rate, were recorded. When cough paroxysms occurred, each individual cough was counted separately.

Nebulization experiments were performed by placing one Hartley guinea pig into a chamber fitted with the nebulization device. All extracts and compounds were resuspended in 10% Methanol in PBS (Vehicle). The first day of the experiment consisted of nebulizing the vehicle for 10 min and recording coughs for 20 min. After a 2-day rest period, each guinea pig received 1 mL of each extract (1 mL at 4 or 20 mg/mL) or 1 mL of sulfolipid-1 (250 μg/ml final). Once all treatment groups were delivered over the course of the experiment, a 2-day waiting period occurred, followed by a treatment of 0.4 M citric acid (positive control). Coughs recorded by the instrument were simultaneously verified by direct observation.

Aerosol infection and Guinea Pig Plethysmography

Mtb cultures in 7H9 broth were centrifuged and the pellet was washed 3 times with PBS. The pellet was then resuspended in PBS and centrifuged (Sorvall Legend X1) at 500 rpm to remove clumps. To generate a single cell suspension, the bacteria-containing supernatant was then sonicated in a water bath using an ultrasonic processor with cup horn attachment (Cole Palmer) at 90% intensity for 15 s. Bacteria were then diluted in PBS to yield an OD_{600} of 0.1 (~3×10^7 CFU/ml), the bacterial suspension placed into the nebulization chamber of a GlasCol aerosolization unit and guinea pigs were infected with ~100-200 CFU. At day 0, the right lung from 3 guinea pigs of each treatment group were homogenized and plated to determine initial CFU. For whole body plethysmography, guinea pigs were placed individually into the nebulization chamber for 24 hr. Depending on the experiment, this was done at either 2, 4 and 6 weeks, or 3- and 6-weeks post infection. For the comparison of wild-type, Mtb*Δstf0* and Mtb*Δstf0::stf0*, infections were staggered to allow for exact comparison of time points. At the completion of the study, the right lung was homogenized to determine CFU and the left lung was fixed in 10% formalin for 16 hr for histology.

Histology

Lungs were first fixed in formalin for 16 hr. The formalin was replaced by PBS, lung tissue was embedded in paraffin and sectioned. Sections (5 μm) were then placed on glass slides and stained with hematoxylin and eosin. The sections in their entirety were scanned at 40x magnification using a NanoZoomer S60 digital slide scanner. For quantification of inflammation, an individual blinded to the samples used ImageJ to identify regions of inflammation and calculate percent inflammation by dividing the inflamed area by the total lung area.

Synthesis of trehalose-2-sulfate (T2S)

A 5 mL flame-dried reaction vial was purged under argon. To a solution of 52 mg 4,6,4',6'-dibenzylidene α,α-D-trehalose (0.1 mmol) (Guiard et al., 2008) in pyridine (0.06M) was added 3 equivalents 25 mg SO_3·pyridine in dimethylformamide (0.5M) dropwise. The reaction was stirred at room temperature for 24 hr. The solvent was then removed under reduced pressure and left to dry overnight under high vacuum. The desired product was separated from starting material and its regioisomer via high performance liquid chromatography (H_2O (0.1% trifluoroacetic acid (TFA):acetonitrile). The resulting fractions were combined and neutralized with 5% $NaHCO_3$ and solvent was removed under reduced pressure. The dimethoxytrityl (DMT) protecting group was cleaved during concentration of the fractions. The remaining water was removed via lyophilization and the resulting mixture contained the product and TFA salt. The TFA salt was removed via a double resin exchange procedure. The obtained mixture was dissolved in water, and added to the Dowex 50WX8 resin (H^+ form, 10 equiv) in a scintillation vial. After stirring for 2 hr, the resin was filtered off and dried via lyophilization overnight. The product was again dissolved in water along with the Dowex 50WX8 resin (Na^+ form, 10 equiv). The mixture was stirred for 2 hr. After filtration off the resin, the desired product trehalose-2-sulfate (T2S) was dried via lyophilization overnight as a white crystalline solid in 8.4 mg, 19% overall yield. ^{1}H NMR (500 MHz, CD_3OD): 5.50 (d, J = 3.6 Hz, 1H), 5.10 (d, J = 3.7 Hz, 1H), 4.18 (dd, J = 9.8, 3.6 Hz, 1H), 4.04 (ddd, J = 10.2, 4.9, 2.5 Hz, 1H), 3.94 (t, J = 9.3 Hz, 1H), 3.90 – 3.74 (m, 4H), 3.72 – 3.65 (m, 2H), 3.48 (dd, J = 9.7, 3.8 Hz, 1H), 3.46 – 3.40 (m, 1H), 3.34 (dd, J = 8.6, 1.8 Hz, 1H). HPLC-MSD: cal'd for [$C_{12}H_{22}O_{14}S$-H^+] 421.07, found: 421.10.

QUANTIFICATION AND STATISTICAL ANALYSIS

Statistical analysis was performed using GraphPad Prism. For *in vitro* intracellular Ca^{2+} assays, either Student's t test for pairwise comparisons, or analysis of variance with Kruskal-Wallace (Fluo-4) or Friedman's test (Fura-2) with correction for multiple comparisons were used. For the restimulation experiment, the Mtb*Δstf0* and restimulated cells were compared using the paired Student's t test. For the SL-1 dose response, the normalized average maximum fluorescence change at each dose was plotted and the EC_{50} was determined using a nonlinear curve fit. For guinea pig experiments with nebulization of Mtb extracts or pure SL-1, Friedman's test for matched, non-parametric data with correction for multiple comparisons was used. For Mtb infected guinea pig cough experiments, the non-parametric Mann-Whitney U test or the Kruskal-Wallis test with correction for multiple comparisons was performed. To identify outliers in animal studies both Dixon's Q test ($Q_{99\%}$) and Grubb's outlier test (alpha 0.01) were used, and an outlier was only removed from the statistical analysis if it was identified by both methods.

DATA AND CODE AVAILABILITY

This study did not generate any unique datasets or code. All other data supporting the findings of this study are available in the manuscript or the supplementary materials and available from the authors upon reasonable request.

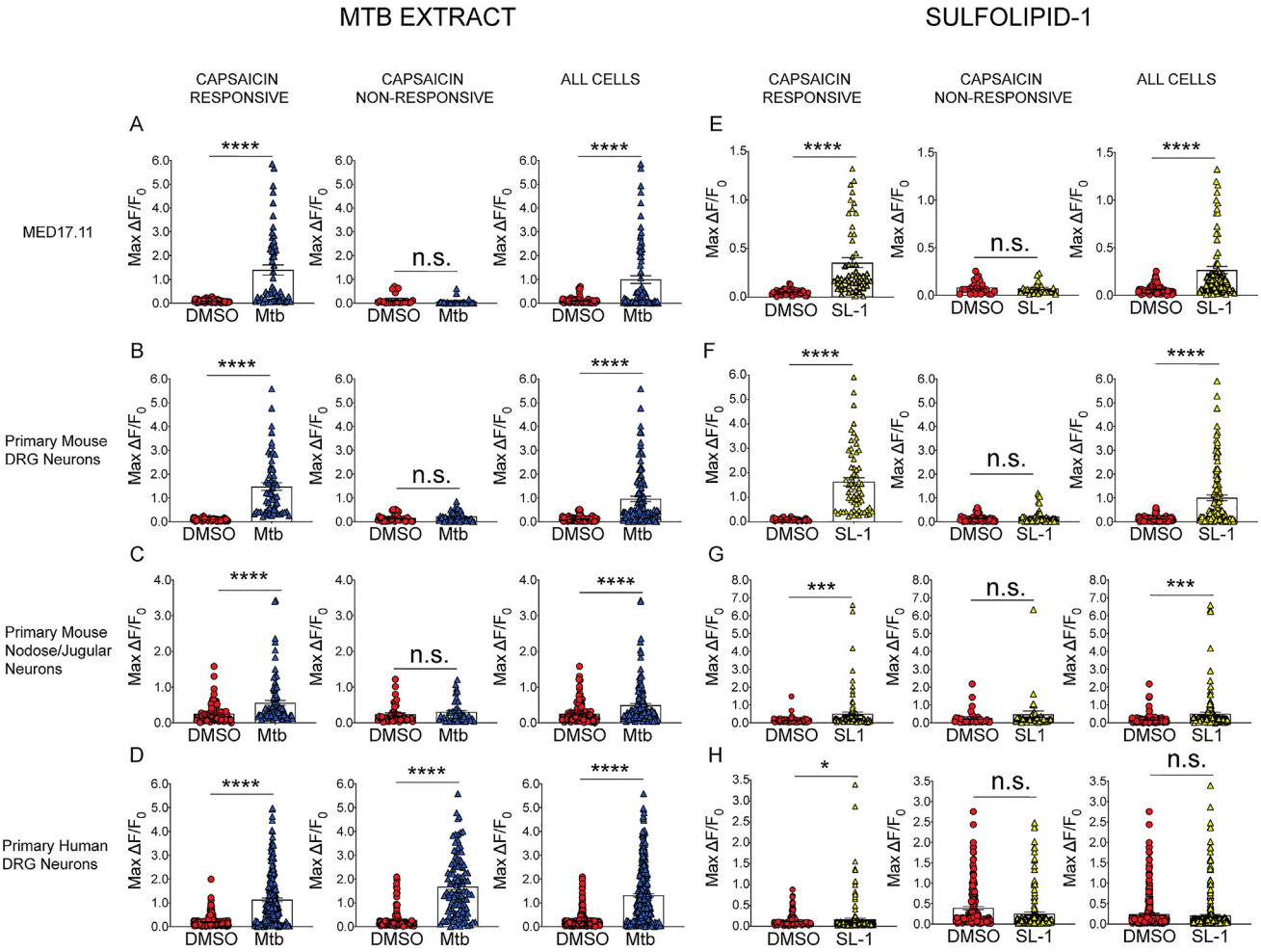

Figure S1. Mtb Extract and SL-1 Increases Intracellular [Ca^{2+}] in Nociceptive Neuron, Related to Figures 2 and 4

(A-D). Fura-2 intracellular calcium assays (Ex 340/380, Em 510 nm) using MED17.11 cells (A), primary mouse DRG neurons (B), primary mouse nodose/jugular ganglia neurons (C) and primary human DRG neurons (D) exposed to Mtb extract. The maximum change in Fura-2 fluorescence ratio for capsaicin responsive (TRPV1+) neurons, capsaicin unresponsive (TRPV1-) and all cells in an experiment (minimum 50 cells) (A-C) are shown. (E-H) Fura-2 intracellular calcium assays using MED17.11 cells (E), primary mouse DRG neurons (F), primary mouse nodose/jugular ganglia neurons (G) and primary human DRG neurons (H) exposed to SL-1. For experiments with mouse (MED17.11, DRG and nodose/jugular) neurons, representative experiments of at least 3 are shown. For human DRG neurons, shown is the combined data from two donors. Error bars represent SEM. *p < 0.05, *** p < 0.001, ****p < 0.0001 by paired Student's t test.

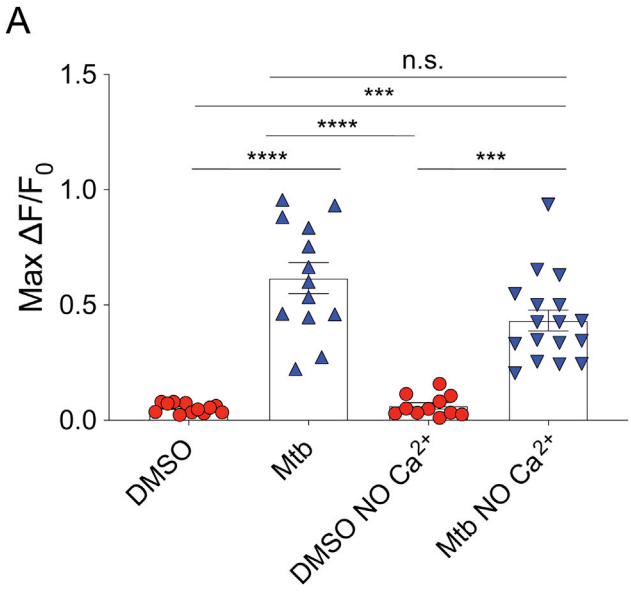

Figure S2. Effect of Extracellular Ca^{2+} on Intracellular [Ca^{2+}] Responses of MED17.11 Neurons to Mtb Extract, Related to Figure 2

(A) Quantification of the average max $\Delta F/F_0$ MED17.11 cells loaded with Fura-2 and treated with vehicle (DMSO) or WT Mtb extract (0.4 mg/mL final). Cells were placed in HHBSS with (DMSO and Mtb extract) or without Ca^{2+} (DMSO NO Ca^{2+} and Mtb NO Ca^{2+}). ***$p < 0.0005$, ****$p < 0.0001$ by Kruskal-Wallace test.

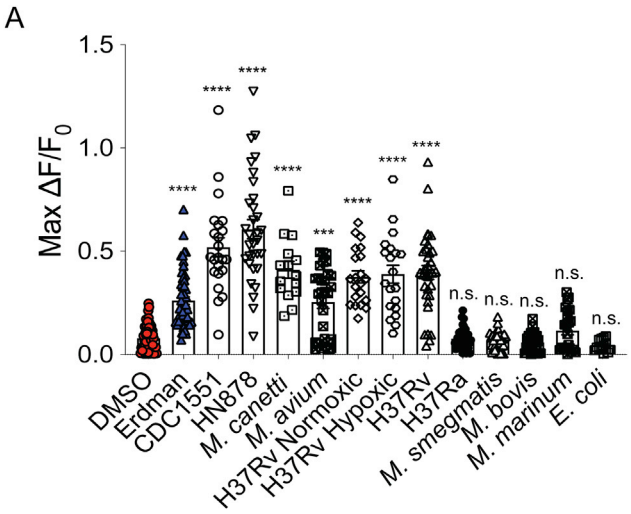

Figure S3. Intracellular Ca^{2+} Changes of MED17.11 Neurons in Response to Various Bacterial Organic Extracts, Related to Table 2

(A) Quantification of the average max $\Delta F/F_0$ MED17.11 cells loaded with Fluo-4 and treated with vehicle (DMSO) or organic extracts from a variety of bacterial species (0.4 mg/mL final). ***$p < 0.001$, ****$p < 0.0001$ by Kruskal-Wallace test.

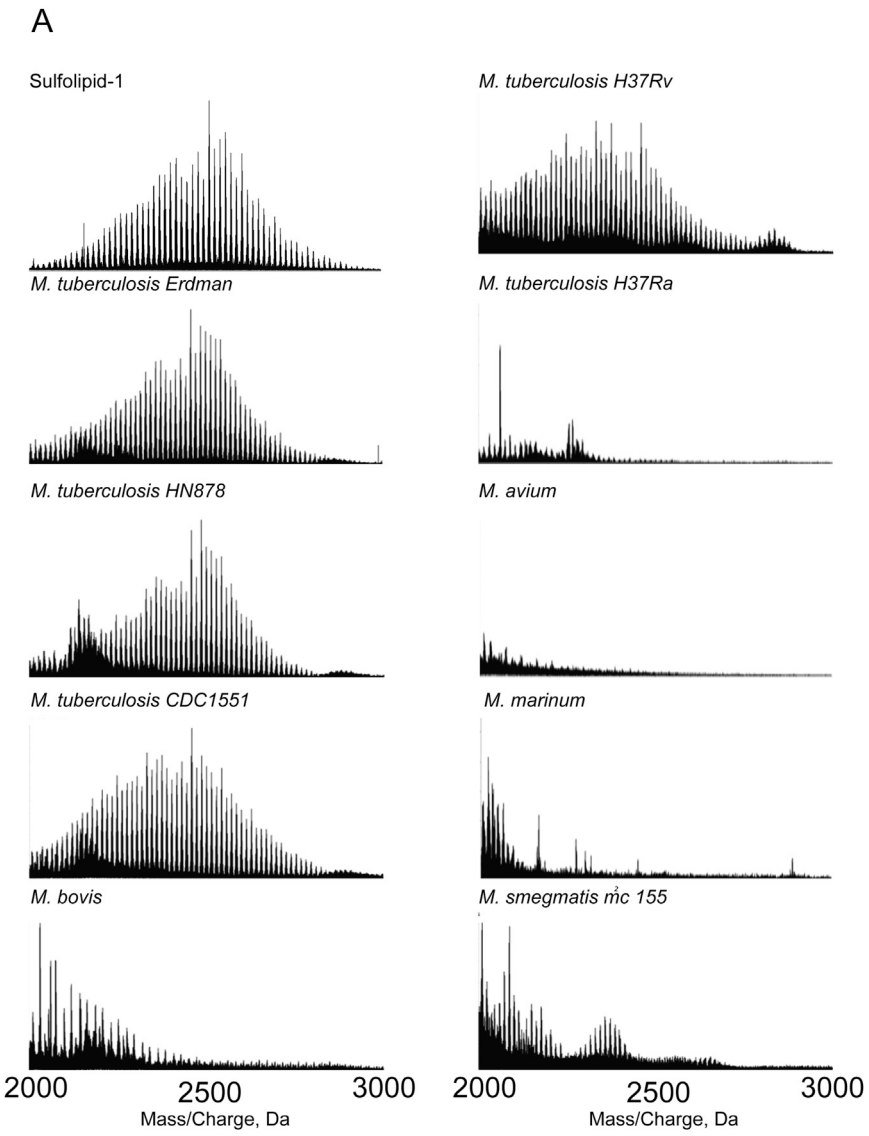

Figure S4. Mass Spectrometry of Mycobacterial Extracts, Related to Table 2

(A) Mass spectra from 2000 – 3000 m/z of pure SL-1 and mycobacterial extracts.

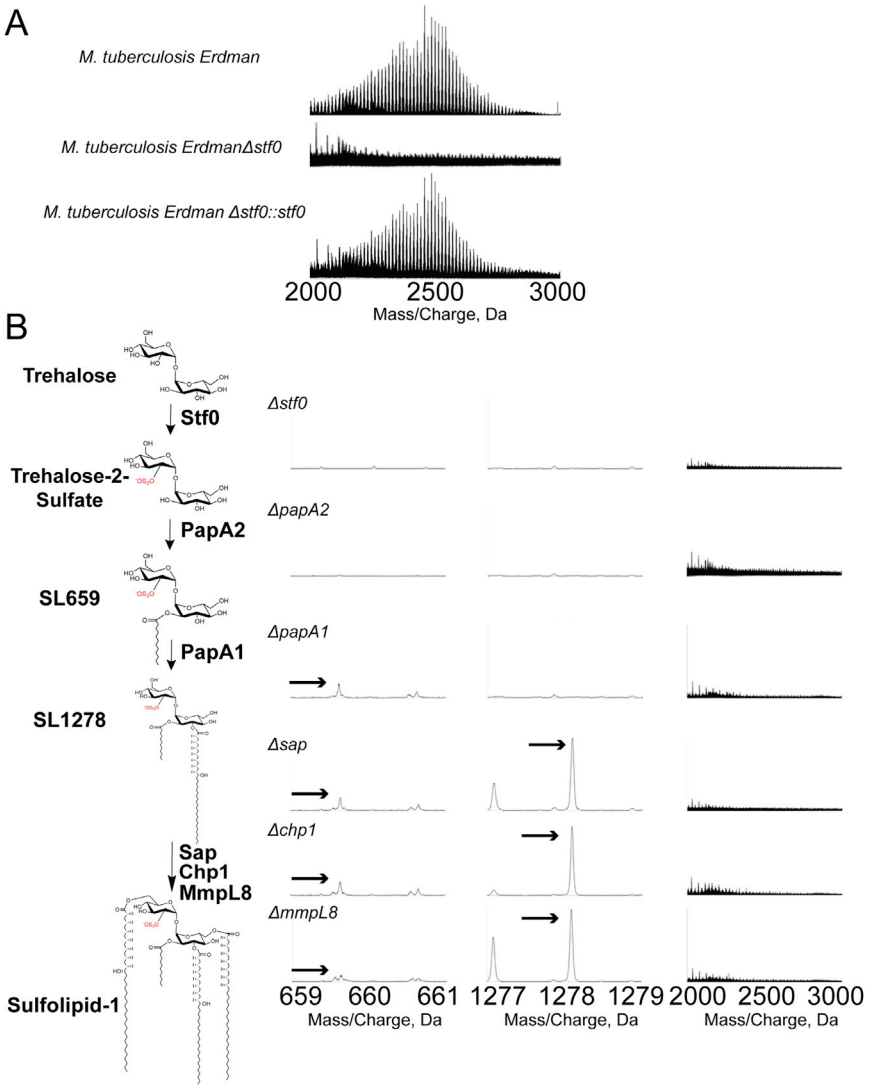

Figure S5. Mass Spectrometry of SL-1 Pathway Mutants, Related to Figure 3

(A) Mass spectra from 2000 – 3000 m/z of Mtb WT, Mtb*Δstf0* and Mtb *Δstf0::stf0*. (B) Mass spectra of Mtb mutants in the SL-1 synthesis pathway in the regions of 659-661 m/z (for SL659), 1277-1279 m/z (for SL1278) and 2000-3000 m/z (for SL-1). Stf0 (Trehalose 2-sulfotransferase; Rv0295c), PapA2 (Polyketide synthase-associated protein A2; acyltransferase; Rv3820c), PapA1 (Polyketide synthase-associated protein A1; acyltransferase; Rv3824c), Sap (Sulfolipid-1-addressing protein; sulfolipid exporter; Rv3821), Chp1 (Cutinase-like hydrolase protein; SL1278 acyltransferase; Rv3822), MmpL8 (Sulfolipid-1 exporter, Rv3823c). Arrows identify SL659 and SL1278.

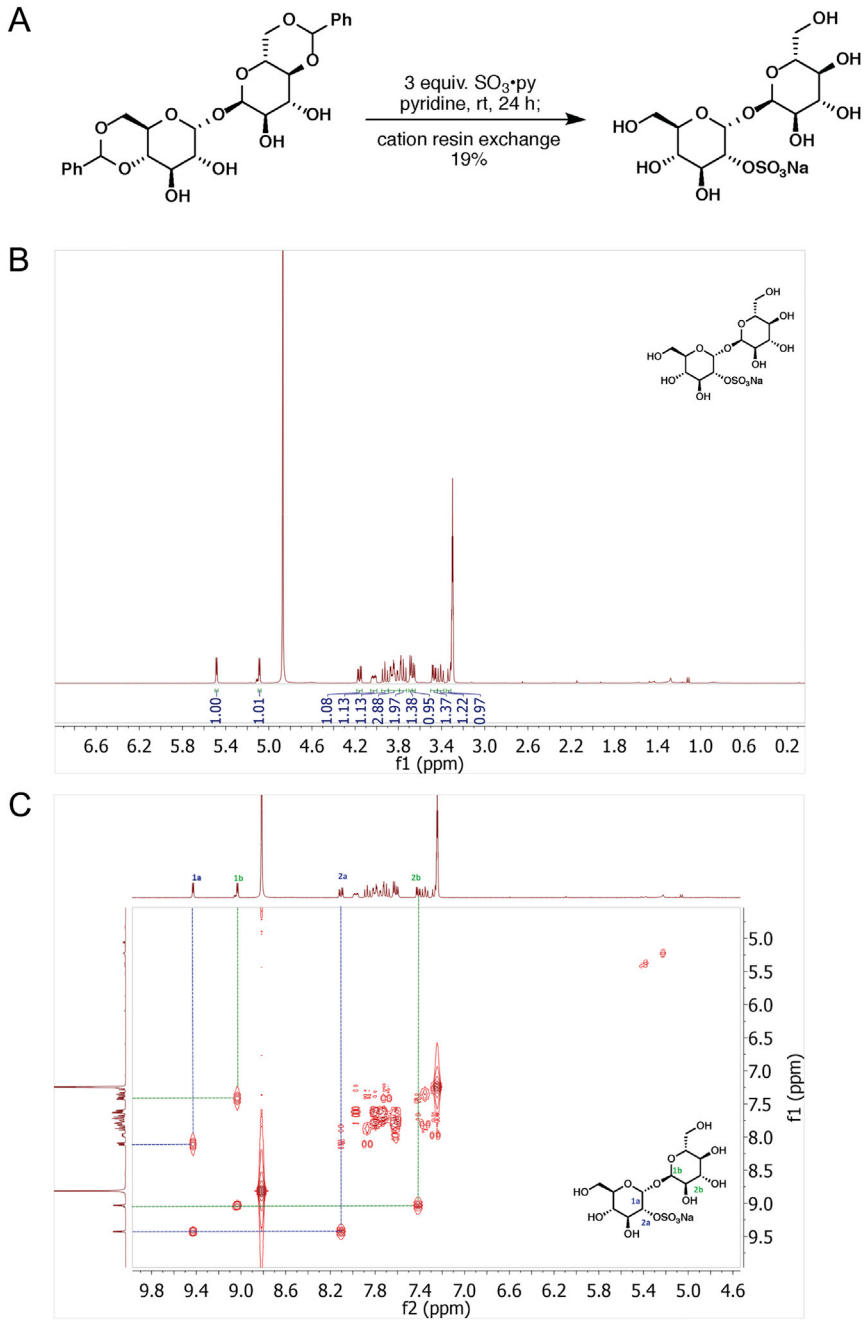

Figure S6. Synthesis of Trehalose-2-Sulfate and Corresponding NMR Spectra, Related to Figure 3

(A) Synthesis of trehalose-2-sulfate from trehalose. (B) ^{1}H NMR spectrum. (C) COSY NMR spectrum.